

1 **Determinants of *de novo* B cell responses to drifted epitopes in post-vaccination**  
2 **SARS-CoV-2 infections**

3 Grace E. Quirk<sup>1,\*</sup>, Marta V. Schoenle<sup>2,\*^</sup>, Kameron L. Peyton<sup>2</sup>, Jennifer L. Uhrlaub<sup>2</sup>,  
4 Branden Lau<sup>3</sup>, Jefferey L. Burgess<sup>4</sup>, Katherine Ellingson<sup>5</sup>, Shawn Beitel<sup>4</sup>, James  
5 Romine<sup>4</sup>, Karen Lutrick<sup>6</sup>, Ashley Fowlkes<sup>7</sup>, Amadea Britton<sup>7</sup>, Harmony L. Tyner<sup>8</sup>, Alberto  
6 J. Caban-Martinez<sup>9</sup>, Allison Naleway<sup>10</sup>, Manjusha Gaglani<sup>11</sup>, Sarang Yoon<sup>12</sup>, Laura  
7 Edwards<sup>13</sup>, Lauren Olsho<sup>13</sup>, Michael Dake<sup>14</sup>, Bonnie J. LaFleur<sup>15</sup>, Janko Ž. Nikolich<sup>15,16</sup>,  
8 Ryan Sprissler<sup>3</sup>, Michael Worobey<sup>1,15,#</sup>, and Deepta Bhattacharya<sup>2,15,17,#</sup>

9 <sup>1</sup> Department of Ecology and Evolutionary Biology, University of Arizona, Tucson, AZ,  
10 USA

11 <sup>2</sup>Department of Immunobiology, University of Arizona College of Medicine, Tucson, AZ,  
12 USA

13 <sup>3</sup> University of Arizona Genomics Core and the Arizona Research Labs, University of  
14 Arizona Genetics Core, University of Arizona, Tucson, AZ, USA

15 <sup>4</sup> Mel and Enid Zuckerman College of Public Health, University of Arizona, Tucson,  
16 Arizona, USA

17 <sup>5</sup> Department of Epidemiology and Biostatistics, Zuckerman College of Public Health,  
18 University of Arizona, Tucson

19 <sup>6</sup> College of Medicine-Tucson, University of Arizona, Tucson, Arizona, USA

20 <sup>7</sup> National Center for Immunization and Respiratory Diseases, Centers for Disease  
21 Control and Prevention, Atlanta, GA

22 <sup>8</sup> St. Luke's Regional Health Care System, Duluth, Minnesota, USA

23 <sup>9</sup> University of Miami, Leonard M. Miller School of Medicine, Miami, FL, USA

24 <sup>10</sup> Kaiser Permanente Northwest Center for Health Research, Portland, Oregon, USA

25 <sup>11</sup> Baylor Scott & White Health and Texas A&M University College of Medicine, Temple,  
26 Texas, USA

27 <sup>12</sup> Rocky Mountain Center for Occupational and Environmental Health, Department of  
28 Family and Preventive Medicine, University of Utah Health, Salt Lake City, Utah, USA

29 <sup>13</sup> Abt Associates, Rockville, Maryland, USA

30 <sup>14</sup> Office of the Senior Vice-President for Health Sciences, University of Arizona,  
31 Tucson, AZ, USA

32 <sup>15</sup> BIO5 Institute, University of Arizona, Tucson, AZ, USA

33 <sup>16</sup> University of Arizona Center on Aging, University of Arizona College of Medicine,  
34 Tucson, AZ, USA

35 <sup>17</sup> Department of Surgery, University of Arizona College of Medicine, Tucson, AZ, USA

36 \*These authors contributed equally

37 #These authors contributed equally

- 38    ^Current address: Department of Microbiology and Immunology, Cornell University,  
39    Ithaca, NY
- 40    Address correspondence to: [deeptab@arizona.edu](mailto:deeptab@arizona.edu)

41 **Summary:**

42 Vaccine-induced immunity may impact subsequent *de novo* responses to drifted  
43 epitopes in SARS-CoV-2 variants, but this has been difficult to quantify due to the  
44 challenges in recruiting unvaccinated control groups whose first exposure to SARS-  
45 CoV-2 is a primary infection. Through local, statewide, and national SARS-CoV-2  
46 testing programs, we were able to recruit cohorts of individuals who had recovered from  
47 either primary or post-vaccination infections by either the Delta or Omicron BA.1  
48 variants. Regardless of variant, we observed greater Spike-specific and neutralizing  
49 antibody responses in post-vaccination infections than in those who were infected  
50 without prior vaccination. Through analysis of variant-specific memory B cells as  
51 markers of *de novo* responses, we observed that Delta and Omicron BA.1 infections led  
52 to a marked shift in immunodominance in which some drifted epitopes elicited minimal  
53 responses, even in primary infections. Prior immunity through vaccination had a small  
54 negative impact on these *de novo* responses, but this did not correlate with cross-  
55 reactive memory B cells, arguing against competitive inhibition of naïve B cells. We  
56 conclude that dampened *de novo* B cell responses against drifted epitopes are mostly a  
57 function of altered immunodominance hierarchies that are apparent even in primary  
58 infections, with a more modest contribution from pre-existing immunity, perhaps due to  
59 accelerated antigen clearance.

60 **Introduction:**

61           Within a year of the discovery of SARS-CoV-2 as the etiological agent of COVID-  
62 19<sup>1</sup>, highly effective vaccines were developed and administered. Leading this class  
63 were the monovalent mRNA vaccines BNT162b2 and mRNA-1273 encoding the  
64 ancestral Spike protein, both of which achieved ~95% efficacies in preventing  
65 symptomatic illness<sup>2,3</sup>. Other vaccine platforms also achieved high efficacies, especially  
66 against severe illness and hospitalization<sup>4-8</sup>. Since the initial results of these clinical  
67 trials, however, the protective capacity of these vaccines has declined<sup>9-12</sup>. This drop in  
68 vaccine effectiveness is due to both waning of antibodies and viral evolution and escape  
69 from vaccine-induced neutralizing antibodies, which are the best-known correlates of  
70 protection<sup>13,14</sup>. While the known genetic diversity of SARS-CoV-2 was quite modest  
71 through most of 2020<sup>15</sup>, new variants with enhanced transmissibility and/or neutralizing  
72 antibody escape mutations have since emerged and sequentially swept to global  
73 dominance<sup>12,16-24</sup>. As of this writing, the dominant circulating variant is Omicron, which  
74 comprises sublineages that contain Spike protein mutations located within most known  
75 neutralizing antibody epitopes<sup>25</sup>. A key issue that will define both protection against  
76 infections and the strategy underlying updates to the vaccines is the extent to which  
77 pre-existing vaccine-induced immunity protects against heterologous challenges like  
78 Omicron.

79           B cell responses following mRNA COVID-19 vaccination are characterized by  
80 exceptionally long-lived germinal center reactions that persist for months while  
81 continuously improving the breadth and affinity of antibodies<sup>26-29</sup>. Cells exiting the  
82 germinal center carry affinity-enhancing mutations and can become long-lived antibody-

83 secreting plasma cells or memory B cells<sup>30</sup>. Depending on the subset of memory B cell,  
84 re-exposures to antigen trigger differentiation to new plasma cells or germinal center  
85 reactions<sup>31–34</sup>. After antigens from infection or vaccine antigens have been cleared,  
86 long-lived plasma cells and memory B cells persist to maintain humoral immunity.

87       While these features protect against homologous SARS-CoV-2 infections, it is  
88 more difficult to predict the nature of responses to subsequent heterologous infections  
89 or vaccines. Due to their expanded pre-existing numbers and intrinsic signaling and  
90 transcriptional differences relative to naive B cells, memory B cells rapidly mount  
91 responses that are of greater magnitude than those of naïve primary responses<sup>35–40</sup> to  
92 either initial infection or vaccination. Because of these properties, memory B cells that  
93 react to epitopes conserved between the original and secondary challenges could  
94 dominate the response to heterologous infections or vaccines<sup>41–43</sup>. If antigen and T cell  
95 help are limiting, memory B cells might then outcompete naive B cells and new primary  
96 antibody responses aimed at the new variant-specific epitopes. This phenomenon,  
97 known as antigenic imprinting or “original antigenic sin”<sup>44</sup>, can be beneficial if antibodies  
98 against the conserved epitopes are protective. However, recall responses to  
99 heterologous pathogens can potentially be neutral or even detrimental if antibodies  
100 targeting these conserved epitopes are not protective and variant-specific primary  
101 responses are competitively inhibited<sup>45</sup>. As an example of the phenomenon, pre-existing  
102 common coronavirus-specific memory B cells compose a majority of the early response  
103 to SARS-CoV-2, but primary responses to epitopes unique to SARS-CoV-2 are readily  
104 observed later<sup>26,46,47</sup>. Whether common coronavirus immunity is helpful, harmful, or  
105 neutral for *de novo* responses to SARS-CoV-2 is unknown.

106           In influenza infections, antigenic imprinting has been proposed to explain the  
107 age-associated differential in morbidity and mortality based on influenza subtype  
108 exposure history<sup>48–51</sup>. The various hemagglutinin (HA) subtypes of influenza A virus fall  
109 into one or the other of two phylogenetically distinct HA “groups” (group 1 or group 2).  
110 Individuals have the highest antibody titers against influenza strains encountered early  
111 in life, and they experience enhanced protection against influenza strains that are within  
112 the same HA group as their primary infection strain compared to heterosubtypic  
113 infections from the group that is mismatched to their first childhood infection. Previous  
114 work has shown that childhood exposure to H1N1 (group 1 hemagglutinin (HA)) affords  
115 protection against other group 1 HAs, such as H5N1. The same is true for individuals  
116 with group 2 HAs, whereby childhood H3N2 infection affords protection against H7N9.  
117 Conversely, individuals with group 1 imprinting experience an increase in mortality when  
118 faced with a group 2 influenza virus infection, such as that observed for H7N9  
119 infections<sup>48,51</sup>.

120           Though pre-existing immunity can certainly impact primary responses to  
121 heterologous antigens, other mechanisms can also limit antibody responses to drifted  
122 epitopes. Epitopes that were previously immunodominant for antibody responses do not  
123 necessarily remain so once mutated, irrespective of prior immunity<sup>52</sup>. There are several  
124 possible mechanistic reasons why not all epitopes are equal for antibody responses.  
125 Factors such as naïve antigen-specific B cell precursor frequency and avidity vary  
126 greatly across epitopes, which in turn correlate with their relative contribution to the  
127 subsequent response<sup>53–57</sup>. Some epitopes can also be biophysically challenging for  
128 antibody binding, such as those sterically blocked by glycan shields or appearing as

129 non-complex ‘smooth’ surfaces to B cells<sup>58,59</sup>. Further, epitopes that mimic self-antigens  
130 also elicit poor responses due to tolerance mechanisms that remove or hamper B cells  
131 from the repertoire that could otherwise respond<sup>60–63</sup>. Finally, V gene usage during  
132 V(D)J recombination that gives rise to B cell receptors is uneven, as some segments  
133 are more heavily utilized than others<sup>64,65</sup>. In turn, this can create ‘holes’ in the repertoire,  
134 rendering some epitopes poorly immunogenic<sup>66</sup>. As SARS-CoV-2 variants of concern  
135 accumulate mutations in antigenic regions, immunodominance might change in ways  
136 that limit responses to drifted epitopes, with or without prior immunity. Thus, it has  
137 remained difficult to examine the degree to which infrequent *de novo* variant-specific  
138 responses in post-vaccination infections and heterologous boosters are due to changes  
139 in immunodominance, antigenic imprinting, or some combination of both<sup>67–75</sup>.

140       Antigenic imprinting has remained nearly impossible to quantify directly and  
141 instead has predominantly relied on historical epidemiological data to make inferences  
142 about biological mechanisms that produce the documented patterns<sup>48,76,77</sup>. The COVID-  
143 19 pandemic presents a unique opportunity to address these questions: it has  
144 encompassed adults with known infection histories and monovalent vaccines that  
145 induce well characterized B cell responses<sup>79,81,83,85</sup> and the emergence of antigenically  
146 distinct viral variants<sup>25,87</sup>. Yet, as immunological histories become more complex and  
147 with very few immunologically naïve adults remaining<sup>82</sup>, the Omicron BA.1 (BA.1, for  
148 short) wave likely represented the final opportunity to recruit robust cohorts of  
149 individuals that meet the key experimental and control criteria. Through voluntary saline-  
150 gargle PCR testing of University of Arizona students, staff, and faculty as part of COVID  
151 mitigation efforts on campus from August 2020 to July 2023; serological testing at 17



152 University of Arizona-managed sites across the state of Arizona; and two CDC-funded  
153 cohorts of essential workers, Arizona Healthcare, Emergency Response, and Other  
154 Essential Workers Surveillance (AZ HEROES)<sup>84</sup> and Research on Epidemiology of  
155 SARS-CoV-2 in Essential Response Personnel (RECOVER)<sup>86</sup>, we recruited  
156 unvaccinated individuals who had recovered from primary Delta (B.1.617.2 or  
157 B.1.617.2-like) or BA.1 (B.1.1.529 or B.1.1.529-like) infections. These cohorts allowed  
158 us to characterize the immunodominance hierarchies for both Delta and BA.1 variants  
159 and directly compare the specificity of antibody responses in unvaccinated individuals  
160 infected by the antigenically drifted viral variants to those generated by post-vaccination  
161 infection by Delta or BA.1. In doing so, we were able to quantify the impact of antigenic  
162 imprinting on *de novo* responses to drifted epitopes.

163

164 **Results:**

165 From our voluntary on-campus testing program at the University of Arizona, we  
166 recruited 37 participants who had tested positive for SARS-CoV-2 infections between  
167 July 1, 2021 and December 1, 2021 despite completion of the primary vaccine series of  
168 monovalent BNT162b2 or mRNA-1273 prior to infection (described in detail in Methods  
169 section). We also recruited 12 individuals who tested positive during this period but had  
170 not received any COVID-19 vaccines. Symptoms reported by participants following  
171 infections were similar between primary and post-vaccination infections; none required  
172 hospitalization. A slightly larger portion of post-vaccination infections were  
173 asymptomatic relative to primary infections (**Figure S1A**), and in general, the duration of  
174 symptoms was significantly shorter in this group relative to those who were  
175 unvaccinated at the time of infection (**Figure S1B**). All recruited individuals who tested  
176 positive by RT-qPCR and had sufficient sequence coverage to assign a lineage had  
177 sequences confirmed to be Delta (**Figure S2A**). During this period, the Delta variant  
178 represented 100% of PCR+ samples on campus that could be assigned a PANGO-  
179 lineage<sup>87</sup>, as determined through viral sequencing of all remnant samples below a Ct  
180 value of 35 (**Figure S2B**). We also selected 71 serum samples as part of our statewide  
181 antibody testing initiative<sup>88</sup> from vaccinated participants who had no self-reported prior  
182 SARS-CoV-2 infections. This cohort was chosen based on matching for age, sex, and  
183 time post-vaccination with our post-vaccination infection group. Characteristics of the  
184 cohorts are listed in **Table 1**.

185 Participants provided blood samples at an average of 75 days (IQR for primary  
186 and post-vaccination infections = 45.8 days, 97.3 days; **Table 1**) after testing positive for

187 SARS-CoV-2 infections and at an average of nine months (IQR for vaccinated only and  
188 post-vaccination infections = 56 days, 317 days; **Table 1**) after their last vaccine dose.  
189 Using plasma from these samples, we first performed live virus neutralization assays on  
190 both an early-pandemic virus representative, (WA-1, from January 2020) or on the  
191 antigenically drifted Delta variant. Against both WA-1 and Delta, post-vaccination Delta  
192 infections led to significantly higher titers of neutralizing antibodies than both primary  
193 infections and vaccinated only controls (**Figure 1A**), indicating a robust recall response.

194 Elevated neutralizing antibody titers in post-vaccination Delta infections could  
195 arise from both memory B cell responses to conserved neutralizing epitopes and  
196 primary responses against new variant-specific epitopes. To begin to determine the  
197 relative specificities of antibodies following Delta infections, we performed ELISAs to  
198 measure the magnitude of the antibody response against Wuhan/Hu1/2019 (hereafter  
199 WuHu1) and Delta Spike antigens. WuHu1 was sampled in December 2019 and is the  
200 SARS-CoV-2 reference sequence; its Spike amino acid sequence is identical to that of  
201 WA-1. We first measured antibodies that bound the receptor binding domain (RBD), as  
202 most neutralizing antibodies target this region<sup>89,90</sup>. Post-vaccination Delta infections led  
203 to elevated RBD-binding antibody titers, both against WuHu1 and Delta, relative to  
204 vaccination only and primary Delta infection controls (**Figure 1B**), again confirming a  
205 robust recall response. As expected, vaccination-only controls showed slightly elevated  
206 titers of WuHu1 RBD-binding antibodies relative to Delta RBD antibodies (**Figure 1B**,  
207 **right panel**). Reciprocally, primary Delta infections led to a skewing towards Delta  
208 RBD-binding antibodies (**Figure 1B, right panel**). Post-vaccination-Delta infections led  
209 to an even ratio of WuHu1:Delta RBD-binding antibodies (**Figure 1B, right panel**),

210 similar to prior studies<sup>91</sup>. Aside from the RBD, neutralizing antibodies can also bind  
211 other regions of the S1 domain of Spike<sup>92–94</sup>. As with RBD, post-vaccination Delta  
212 infections led to an even ratio of antibodies that bound WuHu1 and Delta S1 relative to  
213 vaccination alone or primary Delta infections (**Figure S3**).

214 To more directly assess antibody specificities with single cell resolution in post-  
215 vaccination Delta infections, memory B cells using WuHu1 S1 and Delta S1 antigen  
216 tetramers were quantified by flow cytometry. We focused our analysis on the isotype-  
217 switched CD27+ subset (**Figure 2A and Figure S4**), since few Spike-specific cells are  
218 observed in other memory B cell subsets<sup>95</sup>. Memory B cells that bound Delta S1 only  
219 were observed in both primary infections and in post-vaccination Delta infections,  
220 suggesting that in both cases, *de novo* responses aimed at variant-unique epitopes  
221 were mounted (**Figure 2A-B**). However, the proportions of these cells in PBMCs were  
222 slightly reduced in post-vaccination Delta infections relative to primary Delta infections  
223 (**Figure 2B**). Reciprocally, cross-reactive memory B cells that bound both WuHu1 S1  
224 and Delta S1 were elevated in post-vaccination Delta infections relative to primary Delta  
225 infections (**Figure 2B**), consistent with a robust recall response and antigenic imprinting,  
226 though for a subset of individuals this appears to be more modest. In both primary and  
227 post-vaccination Delta infections, memory B cells that bound Delta S1 uniquely were  
228 rare relative to cross-reactive cells that bound both WuHu1 and Delta S1 (**Figures 2A-**  
229 **B**). Although these data suggest that pre-existing immunity limits new primary  
230 responses, cross-reactive and Delta-specific memory B cells were positively correlated  
231 in post-vaccination Delta infections (**Figure 2C**), arguing against a mechanism of  
232 competitive inhibition between these two cellular compartments.

233           The RBD of Delta contains two non-synonymous point mutations that deviate  
234 from the vaccine sequence: T478K and L452R. The L452R mutation in particular leads  
235 to neutralizing antibody escape<sup>90,96–98</sup>. To estimate the epitope preferences of serum  
236 antibodies further, we produced a Delta RBD protein in which R452 was reverted to  
237 L452. Vaccination led to a response that was skewed toward the L452-containing RBD  
238 (**Figure 3A**, compare to **Figure 1B, middle panel**), confirming the strong antibody bias  
239 and immunodominance of this epitope reported previously<sup>99</sup>. Yet reciprocal skewing to  
240 R452-containing RBD was not observed in primary Delta infections, suggesting that a  
241 new immunogenic epitope is not created by this mutation (**Figure 3A**). Post-vaccination  
242 Delta infections led to a relatively even ratio of antibodies that bound Delta-L452 to  
243 those that reacted to Delta-R452 (**Figure 3A**), perhaps due to boosted levels of  
244 antibodies that bound other conserved sites on RBD and the T478K epitope. We also  
245 produced chimeric WuHu1 S1 proteins in which the Delta N-terminal domain (NTD)  
246 supersite mutations (T19R, G142D, E156-, F157-, R158G) were introduced onto a  
247 WuHu1 background<sup>92–94</sup>. Vaccination only controls showed a relatively even distribution  
248 of antibodies that bound WuHu1 S1 and Delta NTD-WuHu1 S1 (**Figure 3B** compare to  
249 **Figure S3, left panel**). Primary Delta infections, however, were subtly but significantly  
250 skewed towards the Delta NTD (**Figure 3B**). Together, these data demonstrate a  
251 shifting of immunodominance profiles, even in the absence of prior SARS-CoV-2  
252 immunity.

253           To more precisely measure clonal shifts in antibody specificities and  
254 immunodominance than can be achieved by serological assays, we performed LIBRA-  
255 seq using PBMC samples from primary and post-vaccination Delta infections<sup>100</sup>.

256 Streptavidin-phycoerythrin (PE) tetramers were constructed using WuHu1 S1, Delta S1,  
257 Delta RBD, Delta RBD-L452, and Delta NTD-WuHu1-S1, as described in **Figures 1, 3**  
258 and **S3**, each carrying unique oligonucleotide barcodes. PE-binding memory cells were  
259 then enriched and subjected to scRNA/(D)J-seq. Consistent with our serological data  
260 (**Figure 1D**), we observed few memory B cells that bound Delta RBD- and NTD-specific  
261 epitopes (**Figure 3C**). A clear preference for Delta-unique epitopes in the NTD relative  
262 to the RBD was observed within individuals (**Figure 3D**). Within each group, we did not  
263 observe any clear differences in epitope-dependence of somatic mutation frequencies in  
264 memory B cells (**Figure S5A-B**). We did, however, observe a greater frequency of  
265 somatic mutations in Spike-specific memory B cells in the post-vaccination Delta  
266 infection cohort relative to primary Delta infections (**Figure S5C**). Together, these data  
267 suggest a marked shift in antibody specificities in primary Delta variant infections  
268 relative to WuHu1 Spike. This explains in part why responses to at least some drifted  
269 epitopes are not observed, irrespective of prior vaccination.

270         During the course of this work, the heavily mutated Omicron (BA.1) variant  
271 rapidly overtook Delta and swept to global dominance. To define post-vaccination BA.1  
272 responses, we recruited individuals from our voluntary on-campus testing program who  
273 had tested positive for SARS-CoV-2 between January 1 and March 31, 2022, with the  
274 expectation that primary responses would be robust against this more antigenically  
275 distant variant<sup>101</sup>. All individuals for this study who tested positive by PCR had  
276 sequences confirmed to be BA.1 (**Figure S2A**). Individuals with a SARS-CoV-2  
277 infection caused by a Delta variant or other Omicron sublineages were excluded from  
278 the study. Viral genome sequencing of all remnant PCR+ samples on campus during

279 this period below a Ct value of 35 demonstrated that 93.7% of samples that could be  
280 assigned a PANGO-lineage<sup>82,101</sup> were caused by the BA.1 sublineage of Omicron  
281 (**Figure S2B**). To obtain controls for this cohort, some of whom had received 3 doses  
282 of mRNA vaccines, we also recruited a new group of vaccinated individuals who had  
283 never tested positive in our voluntary university testing system and reported no known  
284 prior SARS-CoV-2 infections. After testing plasma for nucleocapsid antibodies as a  
285 marker of prior infection, samples from 5 individuals with titers well above the mean  
286 values seen in verified infections were excluded from further consideration (**Figure S6**).  
287 Relative to both primary and post-vaccination Delta infections, post-vaccination BA.1  
288 infections generally led to fewer symptoms such as wet cough (**Figure S1A**) and shorter  
289 duration of symptoms (**Figure S1B**).

290 We were unable to recruit any unvaccinated individuals on campus who had  
291 experienced BA.1 infections. However, we were able to obtain serum and, for a subset,  
292 PBMC samples from a separate study from the Centers for Disease Control and  
293 Prevention HEROES and RECOVER projects<sup>82,102</sup>, in which 53 individuals met these  
294 criteria (**Table 1**). Neutralizing antibody titers were skewed towards WA-1 in individuals  
295 who had been vaccinated but not infected (**Figure 4A**). Post-vaccination BA.1 infections  
296 led to significantly higher neutralizing antibody titers against BA.1 compared to both  
297 vaccinated controls who had not been infected and primary infections (**Figure 4A**),  
298 consistent with a memory B cell recall response.

299 We next examined binding antibody titers against WuHu1 or BA.1 RBD. Post-  
300 vaccination BA.1 infections led to increased levels of RBD-binding antibodies, both for  
301 WuHu1 and BA.1, relative to the vaccinated only control cohort and primary BA.1

302 infections (**Figure 4B, left and middle panels**). Vaccination alone led to greater RBD  
303 titers against BA.1 than did primary BA.1 infections, despite the many mismatches in  
304 sequence (**Figure 4B, middle panel**). As expected, antibodies from vaccinated only  
305 individuals were skewed towards WuHu1 relative to BA.1 RBD (**Figure 4B, right**  
306 **panel**). Of the few antibodies induced by primary BA.1 infections, we observed a  
307 skewing of specificities towards BA.1 RBD (**Figure 4B, right panel**). Ratios of WuHu1  
308 and BA.1 RBD-binding antibodies in post-vaccination BA.1 infections more closely  
309 resembled vaccinated controls than primary BA.1 infections (**Figure 4B, right panel**).

310 To further evaluate the specificities of antibody responses in post-vaccination  
311 BA.1 infections, we again used antigen tetramers to identify RBD-specific memory B  
312 cells (**Figures S7 and 5A**). As expected, primary BA.1 infections generated a lower  
313 frequency of WuHu1 RBD-specific memory B cells compared to vaccinated controls  
314 (**Figure 5B, left panel**). Unexpectedly, BA.1-specific RBD memory B cells were not  
315 consistently detectable above background in any experimental group, even primary  
316 BA.1 infections (**Figure 5B, middle panel**). These data seem to differ from the modest  
317 skewing of the serological response seen above in primary BA.1 infections (**Figure 4B,**  
318 **right panel**), but can potentially be explained by low overall responses and prior studies  
319 that observed only partial overlap between memory B and antibody-secreting plasma  
320 cell specificities and repertoires<sup>43,103,104</sup>. Instead, most RBD-specific memory B cells  
321 from all cohorts were cross-reactive against WuHu1 and BA.1 RBD (**Figure 5A, 5B,**  
322 **right panel**). Primary BA.1 infections produced numerically fewer cross-reactive RBD  
323 memory B cells than did post-vaccination BA.1 infections (**Figure 5B, right panel**).



324           Given that the overall antibody and memory B cell response to BA.1 RBD was  
325 quite modest (**Figures 4B, 5A-B**), we employed tetramers of full-length Spike trimers of  
326 WuHu1 and BA.1 Spike to capture a greater breadth of memory B cell specificities than  
327 could be observed with RBD tetramers (**Figures 5C**). WuHu1-specific memory B cells  
328 were observed in vaccinated controls and post-vaccination BA.1 infections, but not after  
329 primary BA.1 infections (**Figures 5D, left panel**). We again failed to consistently  
330 observe BA.1-specific memory B cells in any of the groups, including primary BA.1  
331 infections, though a subset of post-vaccination BA.1 infections did appear to generate  
332 such cells well above background levels (**Figure 5D, middle panel**). As with RBD,  
333 cross-reactive Spike-specific memory cells were significantly elevated in post-  
334 vaccination BA.1 infections relative to primary BA.1 infections, but not relative to  
335 vaccinated only controls (**Figure 5D, right panel**). Cross-reactive memory B cells  
336 composed by far the largest portion of SARS-CoV-2 specific responses within all  
337 experimental groups (**Figure S8**).

338           For a subset of primary BA.1 and post-vaccination BA.1 cohorts, we obtained  
339 samples which enabled us to quantify WuHu1, BA.1, and cross-reactive Spike- and  
340 RBD- specific memory B cell frequencies before and after BA.1 infection. Irrespective of  
341 vaccination status, memory B cells that were either WuHu1- or BA.1-RBD-specific  
342 increased in frequency for only a subset of individuals after BA.1 infection (**Figure 6A,**  
343 **left and middle panels**). However, cross-reactive RBD memory B cells consistently  
344 and significantly increased after both primary and post-vaccination BA.1 infections  
345 (**Figure 6A, right panel**). The frequency of cross-reactive Spike memory B cells also  
346 significantly increased after primary BA.1 infections (**Figures 6B, right panel**).

347 To infer potential mechanisms of antigenic imprinting from these samples, we  
348 first correlated pre-infection cross-reactive Spike-specific memory B cells and post-  
349 infection BA.1 Spike-specific memory B cells. A negative correlation could indicate  
350 detrimental imprinting, whereby pre-existing memory B cells outcompete naïve B cells  
351 and inhibit the generation of variant-specific responses. Instead, we observed a slight  
352 positive but non-statistically significant correlation between pre-infection cross-reactive  
353 Spike-specific memory B cells and post-infection BA.1 Spike-specific memory B cells  
354 (**Figure 7A**). Similarly, we observed a non-significant positive correlation between post-  
355 infection cross-reactive Spike-specific memory B cells and post-infection BA.1 Spike-  
356 specific memory B cells (**Figure 7B**).

357 Given that these data do not support a mechanism of competitive inhibition of  
358 naïve B cells by cross-reactive memory B cells, we explored other mechanisms by  
359 which *de novo* responses to drifted epitopes are indirectly suppressed, such as  
360 accelerated viral clearance by neutralizing antibodies and/or T cells. We found a  
361 negative, but non-statistically significant correlation of *de novo* responses with pre-  
362 infection BA.1 neutralizing antibody titers (**Figure 7C**). Similarly, we observed a small  
363 and non-significant negative correlation with pre-infection BA.1 Spike-specific T cell  
364 numbers and post-infection BA.1 Spike memory B cells (**Figure 7D**). The small sample  
365 sizes and variable times of blood sampling prior to infection preclude us from making  
366 definitive conclusions about mechanisms driving antigenic imprinting. Nonetheless, the  
367 data suggest that neutralizing antibody and/or memory T cell-mediated viral clearance  
368 may indirectly underlie suppression of responses to drifted epitopes. This overall impact

369 is quite small relative to the marked changes in antibody immunodominance observed  
370 in even primary BA.1 variant infections, irrespective of prior immunity.

371 **Discussion:**

372           Antigenic imprinting is neither inherently beneficial nor detrimental; rather the  
373 impact of prior immunity is context-dependent<sup>104–106</sup>. For example, pre-existing serum  
374 antibodies can improve and focus *de novo* responses upon reinfection to only mutated  
375 novel epitopes through epitope masking<sup>105–107</sup>. Similarly, *de novo* responses to drifted  
376 epitopes can be improved by pre-existing CD4+ memory T cells in what is classically  
377 known as the hapten-carrier effect<sup>108</sup>. Alternatively, high affinity memory B cells can  
378 competitively inhibit naïve B cells by consuming limited amounts of antigen and T cell  
379 help, leading to a suppression of *de novo* antibody responses<sup>109</sup>. If these memory B  
380 cells target non-protective epitopes, this could in theory leave one worse off than if there  
381 were no prior immunity whatsoever<sup>44,110</sup>. Finally, pre-existing immunity could indirectly  
382 suppress new antibody responses to drifted epitopes simply by clearing away virus and  
383 antigen before naïve B cells can robustly participate.

384           Though neutralizing antibody titers were robust following post-vaccination  
385 infections, our results demonstrated a small negative impact of prior immunity on *de*  
386 *novo* responses to drifted epitopes. Yet we found no evidence to support a mechanism  
387 of competitive inhibition by cross-reactive memory B cells. Though not definitive, our  
388 data instead hint at a role for pre-infection neutralizing antibodies and memory T cells,  
389 suggesting that antigen clearance is the main mechanism by which *de novo* B cell  
390 responses are indirectly suppressed by prior immunity. Indeed, pre-existing neutralizing  
391 antibodies likely accelerate viral clearance<sup>111,112</sup>, and viral and vaccine antigens can  
392 potentially also be cleared by T cells or non-neutralizing antibodies via Fc effector  
393 functions<sup>113–115</sup>. Animal studies offer an attractive way to further test mechanisms of

394 antigenic imprinting on heterologous vaccine and viral infection responses. For  
395 example, genetic tracking studies were used to show robust *de novo* responses to  
396 Omicron boosters in mice previously vaccinated against the ancestral strain. Yet this  
397 required two booster doses, and a small negative impact of prior immunity was  
398 observed in inverse proportion to the antigenic distance between the two  
399 immunizations<sup>101</sup>. Similar results have been reported in other mouse studies<sup>116</sup>. These  
400 systems can thus potentially be used to manipulate specific immune parameters and  
401 measure their contributions to antigenic imprinting in ways that are not possible in  
402 human studies, especially since few immunologically naïve adults remain to serve as  
403 controls.

404 Immunodominance hierarchies can also determine which epitopes are available  
405 to be targeted by antibodies, irrespective of prior immunity. Prior studies, confirmed in  
406 our experiments, showed that a large portion of COVID-19 vaccine-induced antibodies  
407 are aimed at the L452 class 3 epitope<sup>117</sup>. Yet in the post-vaccination Delta cohort, we  
408 observed few antibodies directed at the epitope containing the L452R mutation. Under  
409 the assumption that one immunodominant epitope was being mutated to another, one  
410 might have concluded that the absence of R452-specific antibodies could be explained  
411 by antigenic imprinting. Yet by including a primary infection cohort, we observed that the  
412 Delta variant intrinsically did not elicit detectable antibody responses against the R452  
413 epitope, even with no prior SARS-CoV-2 exposures, consistent with an independent  
414 study<sup>100</sup>. We can instead conclude that Delta shifts antibody immunodominance  
415 hierarchies to instead focus more on epitopes located in the NTD. These types of shifts  
416 in immunodominance preempt any considerations of the impact of antigenic imprinting.

417 The basis and mechanisms of these shifts for SARS-CoV-2 clearly needs more  
418 investigation to determine whether and how best to overcome them.

419 This study spanned a period from the Delta wave through the more antigenically  
420 distinct BA.1 Omicron wave. A central expectation of antigenic imprinting is that the  
421 extent to which prior immunity interferes with *de novo* responses should decrease as  
422 antigenic distance increases<sup>101</sup>. We used the Delta and BA.1 variants to test this  
423 expectation in SARS-CoV-2 and to understand the impacts of antigenic distance on  
424 antigenic imprinting. Despite our prediction, we observe even less of a variant specific  
425 response in post-vaccination BA.1 infections compared to post-vaccination Delta  
426 infections. Much of this can be explained by shifts in immunodominance in which even  
427 primary BA.1 infections elicited few memory B cell responses to drifted epitopes. Yet  
428 longitudinal sampling during BA.1 infections has also shown that viral titers do not reach  
429 the peak levels observed in Delta infections<sup>118</sup>, suggesting that immune responses to  
430 drifted epitopes occur in proportion to need and antigen availability.

431 **Disclosures:** The findings and conclusions in this report are those of the authors and  
432 do not necessarily represent the official position of the Centers for Disease Control and  
433 Prevention.

434

435 **Acknowledgements:** This work was supported by NIH grants R01AI099108 and  
436 R01AI129945 (D.B.) and a research grant from the Arizona Board of Regents (M.W.  
437 and D.B). This project has been funded in part with Federal funds from the National  
438 Institute of Allergy and Infectious Diseases, National Institutes of Health, Department of  
439 Health and Human Services, under Contract No. 75N93021C00015 (M.W.) The  
440 HEROES-RECOVER cohort is supported by the National Center for Immunization and  
441 Respiratory Diseases and the Centers for Disease Control and Prevention (contracts  
442 75D30120R68013 to Marshfield Clinic Research Institute, 75D30120C08379 to the  
443 University of Arizona, and 75D30120C08150 to Abt Associates).

444

445 **Declaration of Interests:** Sana Biotechnology has licensed intellectual property of D.B.  
446 and Washington University in St. Louis. Gilead Sciences has licensed intellectual  
447 property of D.B. and Stanford University. Clade Therapeutics has licensed intellectual  
448 property of D.B. and University of Arizona. D.B. is a co-founder of Clade Therapeutics.  
449 D.B. served on an advisory panel for GlaxoSmithKline. B.J.L. has a financial interest in  
450 Cofactor Genomics, Inc. and Iron Horse Dx. Geneticure Inc. has licensed intellectual  
451 property of R.S. and R.S is a co-founder of Geneticure Inc. M.W. has received  
452 consulting fees from GLG on SARS-CoV-2 and the COVID-19 pandemic.

453

454 **Methods:**

455

456 ***Participant selection***

457 All human studies conducted at The University of Arizona were approved by the  
458 Institutional Review Board for the Human Subjects Protection Program<sup>†</sup>. Individuals who  
459 had participated in the voluntary on-campus saline gargle testing program and had  
460 either never tested positive or had tested positive during the Delta or BA.1 waves were  
461 contacted by email by the program administrators (not the authors on this study) about  
462 willingness to participate in this research study. Participants were provided a link to an  
463 eligibility questionnaire and, once eligibility (no immunosuppressive therapy in the last 5  
464 years and HIV negative) was confirmed, additional demographic questions and a link to  
465 schedule an appointment for blood draws. Written consent was obtained through an  
466 electronic form. All blood draws were performed at the Clinical and Translational  
467 Sciences Center at The University of Arizona. Additional primary and post-vaccination  
468 BA.1 infection samples were acquired from the CDC HEROES-RECOVERS<sup>††</sup>  
469 cohort<sup>82,84</sup>. This study was reviewed by CDC and approved by the institutional review  
470 boards at participating sites or under a reliance agreement with Abt Associates  
471 institutional review board and was conducted consistent with applicable federal law and  
472 CDC policy under 45 C.F.R. part 46, 21 C.F.R. part 56, 42 U.S.C. Sect. 241(d), 5 U.S.C.  
473 Sect. 552a, 44 U.S.C. Sect. 3501 et seq. Methods for the HEROES-RECOVER  
474 Cohorts have been published previously<sup>118</sup>. In summary, cohorts consisted of  
475 health care personnel, first responders, and other essential and frontline workers  
476 in eight U.S. locations across six states. Participants collected weekly nasal



477 swabs which were tested for SARS-CoV-2 viral material by RT-qPCR and  
478 additional swabs were collected and screened upon the onset of any COVID-19–  
479 like illness symptoms. In addition, blood draws were collected at enrollment, then  
480 approximately every 3 months and after immune modifying events such as  
481 vaccination or infection. Vaccination was documented by self-report and verified  
482 by vaccine cards or electronic medical records or state immunization registries.  
483 HEROES-RECOVER participants were selected based on testing positive for SARS-  
484 CoV-2 during Delta or BA.1 waves and having completed a blood draw after infection.

485

#### 486 ***Saline Gargle PCR testing for SARS-CoV-2***

487 As part of Test All, Test Smart, the University of Arizona’s voluntary campus-wide  
488 testing program, University staff, faculty and students had access to SARS-CoV-2 rRT-  
489 PCR tests from August 2020 – July 2023. At testing and collection sites throughout  
490 campus, individuals were given 5 mL of 0.9 % sterile saline (AddiPak 5 mL sterile saline  
491 single use tubes, Teleflex, LLC) and guided to complete three rounds of a 5-second  
492 swish followed by 10 seconds of gargling (adapted from Goldfarb et al.<sup>119</sup>). Samples  
493 were deposited into collection tubes and then screened for SARS-CoV-2 by rRT-PCR.

494

#### 495 ***PBMC and plasma preparation***

496 Twenty milliliters of blood was collected by venipuncture in heparinized Vacutainer  
497 tubes (BD). For PBMCs, 15ml of Ficoll-Paque PLUS (Thermo Fisher Scientific) was  
498 added to 50-ml Leucosep tubes (Greiner) and spun for 1min at 1,000g to transfer the  
499 density gradient below the filter. Twenty milliliters of blood from the heparinized tubes

500 was then poured into the top of the Leucosep tube and spun at 1,000g for 10min at  
501 room temperature with the brake off. The top plasma layer was carefully collected and  
502 frozen at  $-20^{\circ}\text{C}$ , and the remaining supernatant containing PBMCs above the filter was  
503 poured into a new 50-ml conical tube containing 10mL of PBS and spun at 250g for  
504 10min. Cell pellets were resuspended in RPMI media containing 10% FCS and counted  
505 on a Vi-Cell XR (Beckman Coulter). Cells were diluted to a concentration of  $2 \times 10^7$   
506 cells per mL in RPMI media containing 10% FCS. An equal volume of 80% FCS + 20%  
507 dimethyl sulfoxide was added dropwise and inverted once to mix. Suspensions were  
508 distributed at 1ml per cryovial and frozen overnight at  $-80^{\circ}\text{C}$  in Mr. Frosty freezing  
509 chambers (Nalgene). Vials were then transferred to storage in liquid nitrogen.

510

511

### 512 ***ELISA and quantification of antibody titers***

513 Serological assays were performed as previously described<sup>88</sup>. WuHu1 RBD (cat. no.  
514 SPD-C52H3), WuHu1 S1 subdomain of the SARS-CoV-2 S glycoprotein (cat. no. S1N-  
515 C52H3), WuHu1 Spike (cat. no. SPN-C52H9), Delta RBD (cat. no. SPD-C52Hh), Delta  
516 S1 subdomain (cat. no. S1N-C52Hu), Omicron (BA.1) RBD (cat. no. SPD-C522e),  
517 Omicron (BA.1) Spike (cat. no. SPN-C52Hz) and Nucleocapsid (cat. no. NUN-C5227)  
518 were purchased from Acro Biosystems. Chimeric proteins (Delta RBD-L452 and Delta  
519 NTD-WuHu1 S1) were custom synthesized by GenScript. To obtain titers and single-  
520 dilution OD450 values, antigens were immobilized on high-adsorbency 384-well plates  
521 at  $5 \text{ ng mL}^{-1}$ . Plates were blocked with 1% non-fat dehydrated milk extract (Santa Cruz  
522 Biotechnology, sc-2325) in sterile PBS (Thermo Fisher Scientific HyClone PBS,

523 SH2035) for 1 h, washed with PBS containing 0.05% Tween-20 and overlaid for 60 min  
524 with either a single 1:60 dilution or five serial 1:3 dilutions beginning at a 1:60 dilution of  
525 serum. Plates were then washed and incubated for 1 h in 1% PBS and milk containing  
526 anti-human Pan-Ig HRP-conjugated antibody (Jackson ImmunoResearch, 109-035-064)  
527 at a concentration of 1:2,000 for 1 h. Plates were washed with PBS-Tween solution  
528 followed by PBS wash. To develop, plates were incubated in tetramethylbenzidine  
529 (Fisher Scientific) before quenching with 2 N H<sub>2</sub>SO<sub>4</sub>. Plates were read for 450-nm  
530 absorbance on CLARIOstar Plus from BMG Labtech. All samples were also read at  
531 630 nm to detect any incomplete quenching. Any samples above background 630-nm  
532 values were re-run. Area under the curve (AUC) values were calculated in GraphPad  
533 Prism (v9).

534

535

### 536 ***Virus neutralization assays***

537 All live virus assays were performed at Biosafety Level 3 and were approved by the  
538 University of Arizona Institutional Biosafety Committee. SARS-CoV-2, isolate USA-  
539 WA1/2020, was deposited by Dr Natalie J. Thornburg at the Centers for Disease  
540 Control and Prevention and obtained from the World Reference Center for Emerging  
541 Viruses and Arboviruses. Stocks of WA1/2020 SARS-CoV-2 were generated as a single  
542 passage from received stock vial on mycoplasma-negative Vero cells (ATCC CCL-81).  
543 B.1.617.2 (Delta) was received from WRCEVA, strain designation GNL-1205. B.1.1.529  
544 (Omicron) originated from a nasopharyngeal swab collected at the University of Arizona.  
545 It was passaged once on Calu-3 cells and then once on Vero cells to generate a master

546 stock. Viral PANGO-lineage, BA.1.1<sup>119</sup>, was confirmed by Illumina sequencing  
547 (EPI\_ISL\_17886211) of the master stock.

548 Supernatant and cell lysate were combined, subjected to a single freeze–thaw  
549 and then centrifuged at 1,800g for 10min to remove cell debris. For PRNTs for SARS-  
550 CoV-2, Vero cells (ATCC, CCL-81) were plated in 96-well tissue culture plates and  
551 grown overnight. Vero cells were confirmed by PCR to be free of mycoplasma using the  
552 Universal Mycoplasma Detection Kit (ATCC). Serial dilutions of serum samples were  
553 performed in duplicate and incubated with 100 plaque-forming units of SARS-CoV-2 for  
554 1h at 37 °C. Plasma/serum dilutions plus virus were transferred to the cell plates and  
555 incubated for 2h at 37 °C in 5% CO<sub>2</sub> and then overlaid with 1% methylcellulose. After  
556 72h, plates were fixed with 10% neutral buffered formalin for 30min and stained with 1%  
557 crystal violet. Plaques were imaged using an ImmunoSpot Versa plate reader. The most  
558 dilute serum concentration that led to ten or fewer plaques was designated as the  
559 PRNT<sub>90</sub> titer. Input PFU for each experiment was confirmed by plaque assay.

560

### 561 ***Flow cytometry***

562 One milliliter of pre-warmed FBS was added to a frozen cryovial of 10<sup>7</sup> PBMCs, which  
563 was rapidly thawed in a 37°C water bath. Samples were poured into 15 mL conical tubes  
564 containing 5 mL of pre-warmed RPMI with 5% FBS and 1% anti/anti. Tubes were spun  
565 at 250g for 5 min at room temperature.

### 566 **Delta**

567 Supernatants were removed and cell pellets were resuspended in 200 µL of staining  
568 buffer containing 1 µL each of anti-CD38-APC (BioLegend, clone HIT2), anti-CD13-PE-

569 Cy7 (BioLegend, clone WM15), anti-CD21-PE-Dazzle (BioLegend, clone Bu32), anti-  
570 CD19-APC-efluor-780 (Invitrogen, clone HIB19), anti-IgD-PerCP-Cy5.5 (Biolegend,  
571 clone IA6-2), anti-IgM-FITC (Biolegend, clone MHM-88), anti-CD27-BV510 (Biolegend,  
572 clone M-T271), anti-CD11c-Alexa700 (BioLegend, clone Bu15). Staining buffer also  
573 contained Delta-S1-PE and S1-BV421 tetramers.

#### 574 **BA.1**

575 Supernatants were removed and cell pellets were resuspended in 200  $\mu$ L of staining  
576 buffer containing 1  $\mu$ L each of anti-CD38-BV421 (BioLegend, clone HB-7), anti-CD13-  
577 PE-Dazzle 594 (BioLegend, clone WM15), anti-CD21-PerCP Cy 5.5 (BioLegend, clone  
578 Bu32), anti-CD19-APC-efluor-780 (Invitrogen, clone HIB19), anti-IgD-BV510  
579 (Biolegend, clone 11-26c.2a), anti-IgM-FITC (Biolegend, clone MHM-88), anti-CD27-PE  
580 Cy 7 (Biolegend, clone M-T271), anti-CD11c-Alexa700 (BioLegend, clone Bu15). Cells  
581 were stained with live-dead marker, Zombie Yellow (BioLegend) according to  
582 manufacturer's recommendations. Staining buffer also contained BA.1-Spike-PE and  
583 Spike-Alexa Fluor 647 tetramers.

584

585 Antibodies were validated by the manufacturer on human PBMCs. Tetramer reagents  
586 were assembled by mixing 100 $\mu$ g ml<sup>-1</sup> of C-terminal AviTagged S1, Delta S1, WuHu1  
587 Spike, or BA.1 Spike (ACROBiosystems) with 100 $\mu$ g ml<sup>-1</sup> of streptavidin-PE(BioLegend),  
588 streptavidin-BV421 (BioLegend), or streptavidin-Alexa Fluor 647 (BioLegend),  
589 respectively, at a 6:1 molar ratio for S1 or 4:1 molar ratio for Spike, in which  $\frac{1}{5}$  of the  
590 final volume of streptavidin was added every 10 min. S1 and Spike tetramers were  
591 validated by staining Lenti-X 293T cells(Takara Bio) as a negative control or 293T-

592 hACE2-expressing cells (BEI Resources, NR-52511) as a positive control. Lenti-X 293T  
593 cells were confirmed to be free of mycoplasma; 293T-hACE2 cells were maintained in  
594 media containing 1% pen/strep to minimize chances of contamination. PBMC samples  
595 were stained for at least 20 minutes, washed and filtered through 70- $\mu$ m nylon mesh.  
596 Data were analyzed on either a BD LSR2 (tetramer validation only), a Fortessa  
597 cytometer (Delta), or BD Cytex Aurora (BA.1). Data were analyzed using FlowJo  
598 software.

599

### 600 ***Flow cytometry and Fluorescence Activated Cell Sorting***

601 One milliliter of pre-warmed FBS was added to a frozen cryovial of PBMCs and thawed  
602 by pipetting. Samples were added to 15 mL conical tubes containing 10 mL of pre-  
603 warmed RPMI with 20% FBS and 1% anti/anti. Tubes were spun at 1200 RPM for 5  
604 minutes at room temperature. Supernatants were removed and cell pellets were  
605 resuspended in 200  $\mu$ L of staining buffer contained 1  $\mu$ L each of anti-CD19-  
606 BV421(Biolegend, clone HIB19), anti-CD27-FITC(Biolegend, clone O323), anti-CD13-  
607 PE-Cy-7(Biolegend, clone WM15), anti-IgD-APC-Cy-7(Biolegend, clone IA6-2). Staining  
608 buffer also contained either 5 or 2 LIBRA-Seq tetramers: S1-PE(Biolegend, TotalSeq-  
609 C0951\_PE), Delta S1-PE(Biolegend, TotalSeq-C0952\_PE), Delta NTD/S1-  
610 PE(Biolegend, TotalSeq-C0953\_PE), Delta RBD/L452(Biolegend, TotalSeq-  
611 C0954\_PE), and Delta RBD-PE(Biolegend, TotalSeq-C0955\_PE). Biotinylated tetramer  
612 reagents were assembled by mixing 100 $\mu$ g ml<sup>-1</sup> of C-terminal AviTagged S1  
613 (ACROBiosystems), Delta S1 (ACROBiosystems), Delta NTD/S1 (GenScript), Delta  
614 RBD/L452 (Genscript), or Delta RBD (ACROBiosystems) with 100 $\mu$ g ml<sup>-1</sup> of

615 streptavidin-TotalSeq-C-PE (BioLegend) at a 6:1 molar ratio in which  $\frac{1}{5}$  of the final  
616 volume of streptavidin was added every 10 min. Tetramers were validated by staining  
617 Lenti-X 293T cells(Takara Bio) as a negative control or 293T-hACE2-expressing cells  
618 (BEI Resources, NR-52511) as a positive control. Lenti-X 293T cells were confirmed to  
619 be free of mycoplasma; 293T-hACE2 cells were maintained in media containing 1%  
620 pen/strep to minimize chances of contamination. Additionally, TotalSeq-C anti-human  
621 Hashtag antibodies (Biolegend, TotalSeq™-C0251-10) were added to individual  
622 samples and pooled after staining and washing. PBMCs were stained in the dark for 30  
623 minutes at 4°C, washed, pooled and filtered through a 35 µm strainer (Fisher Scientific).  
624 SARS-CoV-2 specific memory B cells (CD19+IgD-IgM-CD27+) as well as non-antigen  
625 specific memory B cells were sorted using a FACSAria II.

626

### 627 ***Single-cell RNA sequencing and analysis***

628 Cells were prepared and processed according to the 10X Genomics Single Cell 5' Dual  
629 Index protocol with Feature Barcoding Technology for Cell Surface Protein and Immune  
630 Receptor Mapping kit (10X Genomics). Reads were processed and aligned using the  
631 10X CellRanger multi pipeline to GRCh38 gex and vdj reference genomes (10X  
632 Genomics). Each sample feature barcode matrix was loaded into R and analyzed  
633 utilizing the Seurat package for gene expression, vdj and antibody capture analysis<sup>120</sup>.  
634 Cell processing was conducted as previously described<sup>100</sup>. Data are available at NCBI  
635 GEO accession number GSE242775.

636

### 637 ***ELISpot Assay***

638 Cryopreserved PBMC ( $5 \times 10^6$ /sample) were thawed in prewarmed RPMI-1640 media  
639 supplemented with L-glutamine + 10% FCS and 300ug DNase. Thawed PBMCs were  
640 rested overnight at 37 °C in X-VIVO™-15 Medium (Lonza) supplemented with 5%  
641 human-AB serum. Cells were stimulated with ~1 nmol of peptide pool corresponding to  
642 spike of Omicron (B.1.1.529) variant (16-mer peptide pools, overlapping by 10 amino  
643 acids (21st century Biochemicals Inc.) on pre-coated human IFN- $\gamma$  ELISpot plates  
644 (Mabtech, Inc.) and developed after 18 hours according to manufacturer instructions.  
645 Spots were imaged and counted using Iris FLUOROsport reader (Mabtech).

646

#### 647 ***Statistical methods***

648 All analyses are listed in the figure legends and were performed in GraphPad Prism 9  
649 and/or the R programming language (v4.0.5).

650

#### 651 **Footnotes**

652 † See 45 C.F.R. part 46; 21 C.F.R. part 56

653 †† This study was reviewed by CDC and approved by the institutional review boards at  
654 participating sites or under a reliance agreement with Abt Associates institutional review  
655 board and was conducted consistent with applicable federal law and CDC policy under  
656 45 C.F.R. part 46, 21 C.F.R. part 56, 42 U.S.C. Sect. 241(d), 5 U.S.C. Sect. 552a, 44  
657 U.S.C. Sect. 3501 et seq.

658

659

660



661 **References**

- 662 1. Novel 2019 coronavirus genome (2020). Virological. <https://virological.org/t/novel->  
663 2019-coronavirus-genome/319.
- 664 2. Baden, L.R., El Sahly, H.M., Essink, B., Kotloff, K., Frey, S., Novak, R., Diemert, D.,  
665 Spector, S.A., Roupshael, N., Creech, C.B., et al. (2021). Efficacy and safety of the  
666 mRNA-1273 SARS-CoV-2 vaccine. *N. Engl. J. Med.* 384, 403–416.  
667 10.1056/NEJMoa2035389.
- 668 3. Polack, F.P., Thomas, S.J., Kitchin, N., Absalon, J., Gurtman, A., Lockhart, S.,  
669 Perez, J.L., Pérez Marc, G., Moreira, E.D., Zerbini, C., et al. (2020). Safety and  
670 Efficacy of the BNT162b2 mRNA Covid-19 Vaccine. *N. Engl. J. Med.* 383, 2603–  
671 2615. 10.1056/NEJMoa2034577.
- 672 4. Sadoff, J., Gray, G., Vandebosch, A., Cárdenas, V., Shukarev, G., Grinsztejn, B.,  
673 Goepfert, P.A., Truyers, C., Fennema, H., Spiessens, B., et al. (2021). Safety and  
674 efficacy of single-dose Ad26.COV2.S vaccine against Covid-19. *N. Engl. J. Med.*  
675 384, 2187–2201. 10.1056/NEJMoa2101544.
- 676 5. Tanriover, M.D., Doğanay, H.L., Akova, M., Güner, H.R., Azap, A., Akhan, S., Köse,  
677 Ş., Erdinç, F.Ş., Akalın, E.H., Tabak, Ö.F., et al. (2021). Efficacy and safety of an  
678 inactivated whole-virion SARS-CoV-2 vaccine (CoronaVac): interim results of a  
679 double-blind, randomised, placebo-controlled, phase 3 trial in Turkey. *Lancet* 398,  
680 213–222. 10.1016/S0140-6736(21)01429-X.

- 681 6. Heath, P.T., Galiza, E.P., Baxter, D.N., Boffito, M., Browne, D., Burns, F.,  
682 Chadwick, D.R., Clark, R., Cosgrove, C., Galloway, J., et al. (2021). Safety and  
683 efficacy of NVX-CoV2373 covid-19 vaccine. *N. Engl. J. Med.* **385**, 1172–1183.  
684 10.1056/NEJMoa2107659.
- 685 7. Voysey, M., Clemens, S.A.C., Madhi, S.A., Weckx, L.Y., Folegatti, P.M., Aley, P.K.,  
686 Angus, B., Baillie, V.L., Barnabas, S.L., Bhorat, Q.E., et al. (2021). Safety and  
687 efficacy of the ChAdOx1 nCoV-19 vaccine (AZD1222) against SARS-CoV-2: an  
688 interim analysis of four randomised controlled trials in Brazil, South Africa, and the  
689 UK. *Lancet* **397**, 99–111. 10.1016/S0140-6736(20)32661-1.
- 690 8. Xia, S., Zhang, Y., Wang, Y., Wang, H., Yang, Y., Gao, G.F., Tan, W., Wu, G., Xu,  
691 M., Lou, Z., et al. (2021). Safety and immunogenicity of an inactivated SARS-CoV-2  
692 vaccine, BBIBP-CorV: a randomised, double-blind, placebo-controlled, phase 1/2  
693 trial. *Lancet Infect. Dis.* **21**, 39–51. 10.1016/S1473-3099(20)30831-8.
- 694 9. Pouwels, K.B., Pritchard, E., Matthews, P.C., Stoesser, N., Eyre, D.W., Vihta, K.-D.,  
695 House, T., Hay, J., Bell, J.I., Newton, J.N., et al. (2021). Effect of Delta variant on  
696 viral burden and vaccine effectiveness against new SARS-CoV-2 infections in the  
697 UK. *Nat. Med.* **27**, 2127–2135. 10.1038/s41591-021-01548-7.
- 698 10. Chen, J., Wang, R., Gilby, N.B., and Wei, G.-W. (2022). Omicron variant  
699 (B.1.1.529): Infectivity, vaccine breakthrough, and antibody resistance. *J. Chem. Inf.*  
700 *Model.* **62**, 412–422. 10.1021/acs.jcim.1c01451.

- 701 11. Tao, K., Tzou, P.L., Nouhin, J., Gupta, R.K., de Oliveira, T., Kosakovsky Pond, S.L.,  
702 Fera, D., and Shafer, R.W. (2021). The biological and clinical significance of  
703 emerging SARS-CoV-2 variants. *Nat. Rev. Genet.*, 1–17. [10.1038/s41576-021-](https://doi.org/10.1038/s41576-021-00408-x)  
704 [00408-x](https://doi.org/10.1038/s41576-021-00408-x).
- 705 12. Dejnirattisai, W., Huo, J., Zhou, D., Zahradník, J., Supasa, P., Liu, C., Duyvesteyn,  
706 H.M.E., Ginn, H.M., Mentzer, A.J., Tuekprakhon, A., et al. (2022). SARS-CoV-2  
707 Omicron-B.1.1.529 leads to widespread escape from neutralizing antibody  
708 responses. *Cell*. [10.1016/j.cell.2021.12.046](https://doi.org/10.1016/j.cell.2021.12.046).
- 709 13. Gilbert, P.B., Montefiori, D.C., McDermott, A.B., Fong, Y., Benkeser, D., Deng, W.,  
710 Zhou, H., Houchens, C.R., Martins, K., Jayashankar, L., et al. (2022). Immune  
711 correlates analysis of the mRNA-1273 COVID-19 vaccine efficacy clinical trial.  
712 *Science* 375, 43–50. [10.1126/science.abm3425](https://doi.org/10.1126/science.abm3425).
- 713 14. Khoury, D.S., Cromer, D., Reynaldi, A., Schlub, T.E., Wheatley, A.K., Juno, J.A.,  
714 Subbarao, K., Kent, S.J., Triccas, J.A., and Davenport, M.P. (2021). Neutralizing  
715 antibody levels are highly predictive of immune protection from symptomatic SARS-  
716 CoV-2 infection. *Nat. Med.* 27, 1205–1211. [10.1038/s41591-021-01377-8](https://doi.org/10.1038/s41591-021-01377-8).
- 717 15. Rausch, J.W., Capoferri, A.A., Katusiime, M.G., Patro, S.C., and Kearney, M.F.  
718 (2020). Low genetic diversity may be an Achilles heel of SARS-CoV-2. *Proc. Natl.*  
719 *Acad. Sci. U. S. A.* 117, 24614–24616. [10.1073/pnas.2017726117](https://doi.org/10.1073/pnas.2017726117).
- 720 16. Volz, E. (2023). Fitness, growth and transmissibility of SARS-CoV-2 genetic  
721 variants. *Nat. Rev. Genet.*, 1–11. [10.1038/s41576-023-00610-z](https://doi.org/10.1038/s41576-023-00610-z).

- 722 17. Wiegand, T., Nemudryi, A., Nemudraia, A., McVey, A., Little, A., Taylor, D.N., Walk,  
723 S.T., and Wiedenheft, B. (2022). The Rise and Fall of SARS-CoV-2 Variants and  
724 Ongoing Diversification of Omicron. *Viruses* 14, 2009. 10.3390/v14092009.
- 725 18. Hill, V., Du Plessis, L., Peacock, T.P., Aggarwal, D., Colquhoun, R., Carabelli, A.M.,  
726 Ellaby, N., Gallagher, E., Groves, N., Jackson, B., et al. (2022). The origins and  
727 molecular evolution of SARS-CoV-2 lineage B.1.1.7 in the UK. *Virus Evol.* 8,  
728 veac080. 10.1093/ve/veac080.
- 729 19. Cao, Y., Song, W., Wang, L., Liu, P., Yue, C., Jian, F., Yu, Y., Yisimayi, A., Wang,  
730 P., Wang, Y., et al. (2022). Characterization of the enhanced infectivity and  
731 antibody evasion of Omicron BA.2.75. *Cell Host Microbe* 30, 1527-1539.e5.  
732 10.1016/j.chom.2022.09.018.
- 733 20. Volz, E., Mishra, S., Chand, M., Barrett, J.C., Johnson, R., Geidelberg, L., Hinsley,  
734 W.R., Laydon, D.J., Dabrera, G., O'Toole, Á., et al. (2021). Assessing  
735 transmissibility of SARS-CoV-2 lineage B.1.1.7 in England. *Nature* 593, 266–269.  
736 10.1038/s41586-021-03470-x.
- 737 21. Cherian, S., Potdar, V., Jadhav, S., Yadav, P., Gupta, N., Das, M., Rakshit, P.,  
738 Singh, S., Abraham, P., Panda, S., et al. (2021). Convergent evolution of SARS-  
739 CoV-2 spike mutations, L452R, E484Q and P681R, in the second wave of COVID-  
740 19 in Maharashtra, India. *bioRxiv*, 2021.04.22.440932. 10.1101/2021.04.22.440932.
- 741 22. Cheng, Y.-W., Chao, T.-L., Li, C.-L., Wang, S.-H., Kao, H.-C., Tsai, Y.-M., Wang,  
742 H.-Y., Hsieh, C.-L., Lin, Y.-Y., Chen, P.-J., et al. (2021). D614G Substitution of

- 743 SARS-CoV-2 Spike Protein Increases Syncytium Formation and Virus Titer via  
744 Enhanced Furin-Mediated Spike Cleavage. MBio, e0058721. 10.1128/mBio.00587-  
745 21.
- 746 23. McCallum, M., Bassi, J., De Marco, A., Chen, A., Walls, A.C., Di Iulio, J., Tortorici,  
747 M.A., Navarro, M.-J., Silacci-Fregni, C., Saliba, C., et al. (2021). SARS-CoV-2  
748 immune evasion by the B.1.427/B.1.429 variant of concern. Science.  
749 10.1126/science.abi7994.
- 750 24. Imai, M., Halfmann, P.J., Yamayoshi, S., Iwatsuki-Horimoto, K., Chiba, S.,  
751 Watanabe, T., Nakajima, N., Ito, M., Kuroda, M., Kiso, M., et al. (2021).  
752 Characterization of a new SARS-CoV-2 variant that emerged in Brazil. PNAS.  
753 10.1073/pnas.2106535118/-/DCSupplemental.
- 754 25. Viana, R., Moyo, S., Amoako, D.G., Tegally, H., Scheepers, C., Althaus, C.L.,  
755 Anyaneji, U.J., Bester, P.A., Boni, M.F., Chand, M., et al. (2022). Rapid epidemic  
756 expansion of the SARS-CoV-2 Omicron variant in southern Africa. Nature 603,  
757 679–686. 10.1038/s41586-022-04411-y.
- 758 26. Sokal, A., Chappert, P., Barba-Spaeth, G., Roeser, A., Fourati, S., Azzaoui, I.,  
759 Vandenberghe, A., Fernandez, I., Meola, A., Bouvier-Alias, M., et al. (2021).  
760 Maturation and persistence of the anti-SARS-CoV-2 memory B cell response. Cell  
761 184, 1201-1213.e14. 10.1016/j.cell.2021.01.050.
- 762 27. Muecksch, F., Weisblum, Y., Barnes, C.O., Schmidt, F., Schaefer-Babajew, D.,  
763 Wang, Z., C Lorenzi, J.C., Flyak, A.I., DeLaitch, A.T., Huey-Tubman, K.E., et al.

- 764 (2021). Affinity maturation of SARS-CoV-2 neutralizing antibodies confers potency,  
765 breadth, and resilience to viral escape mutations. *Immunity*.  
766 10.1016/j.immuni.2021.07.008.
- 767 28. Turner, J.S., O'Halloran, J.A., Kalaidina, E., Kim, W., Schmitz, A.J., Zhou, J.Q., Lei,  
768 T., Thapa, M., Chen, R.E., Case, J.B., et al. (2021). SARS-CoV-2 mRNA vaccines  
769 induce persistent human germinal centre responses. *Nature*. 10.1038/s41586-021-  
770 03738-2.
- 771 29. Kim, W., Zhou, J.Q., Horvath, S.C., Schmitz, A.J., Sturtz, A.J., Lei, T., Liu, Z.,  
772 Kalaidina, E., Thapa, M., Alsoussi, W.B., et al. (2022). Germinal centre-driven  
773 maturation of B cell response to mRNA vaccination. *Nature*, 1–8. 10.1038/s41586-  
774 022-04527-1.
- 775 30. Victora, G.D., and Nussenzweig, M.C. (2022). Germinal centers. *Annu. Rev.*  
776 *Immunol.* 40, 413–442. 10.1146/annurev-immunol-120419-022408.
- 777 31. Seifert, M., Przekopowicz, M., Taudien, S., Lollies, A., Ronge, V., Drees, B.,  
778 Lindemann, M., Hillen, U., Engler, H., Singer, B.B., et al. (2015). Functional  
779 capacities of human IgM memory B cells in early inflammatory responses and  
780 secondary germinal center reactions. *Proc. Natl. Acad. Sci. U. S. A.* 112, E546-55.  
781 10.1073/pnas.1416276112.
- 782 32. Dogan, I., Bertocci, B., Vilmont, V., Delbos, F., Mégret, J., Storck, S., Reynaud, C.-  
783 A., and Weill, J.-C. (2009). Multiple layers of B cell memory with different effector  
784 functions. *Nat. Immunol.* 10, 1292–1299. 10.1038/ni.1814.

- 785 33. Pape, K.A., Taylor, J.J., Maul, R.W., Gearhart, P.J., and Jenkins, M.K. (2011).  
786 Different B cell populations mediate early and late memory during an endogenous  
787 immune response. *Science* 331, 1203–1207. 10.1126/science.1201730.
- 788 34. Zuccarino-Catania, G.V., Sadanand, S., Weisel, F.J., Tomayko, M.M., Meng, H.,  
789 Kleinstein, S.H., Good-Jacobson, K.L., and Shlomchik, M.J. (2014). CD80 and PD-  
790 L2 define functionally distinct memory B cell subsets that are independent of  
791 antibody isotype. *Nat. Immunol.* 15, 631–637. 10.1038/ni.2914.
- 792 35. Horikawa, K., Martin, S.W., Pogue, S.L., Silver, K., Peng, K., Takatsu, K., and  
793 Goodnow, C.C. (2007). Enhancement and suppression of signaling by the  
794 conserved tail of IgG memory-type B cell antigen receptors. *J. Exp. Med.* 204, 759–  
795 769. 10.1084/jem.20061923.
- 796 36. Waisman, A., Kraus, M., Seagal, J., Ghosh, S., Melamed, D., Song, J., Sasaki, Y.,  
797 Classen, S., Lutz, C., Brombacher, F., et al. (2007). IgG1 B cell receptor signaling is  
798 inhibited by CD22 and promotes the development of B cells whose survival is less  
799 dependent on Ig alpha/beta. *J. Exp. Med.* 204, 747–758. 10.1084/jem.20062024.
- 800 37. Engels, N., König, L.M., Heemann, C., Lutz, J., Tsubata, T., Griep, S., Schrader, V.,  
801 and Wienands, J. (2009). Recruitment of the cytoplasmic adaptor Grb2 to surface  
802 IgG and IgE provides antigen receptor-intrinsic costimulation to class-switched B  
803 cells. *Nat. Immunol.* 10, 1018–1025. 10.1038/ni.1764.
- 804 38. Kometani, K., Nakagawa, R., Shinnakasu, R., Kaji, T., Rybouchkin, A., Moriyama,  
805 S., Furukawa, K., Koseki, H., Takemori, T., and Kurosaki, T. (2013). Repression of

- 806 the transcription factor Bach2 contributes to predisposition of IgG1 memory B cells  
807 toward plasma cell differentiation. *Immunity* 39, 136–147.  
808 10.1016/j.immuni.2013.06.011.
- 809 39. Bhattacharya, D., Cheah, M.T., Franco, C.B., Hosen, N., Pin, C.L., Sha, W.C., and  
810 Weissman, I.L. (2007). Transcriptional profiling of antigen-dependent murine B cell  
811 differentiation and memory formation. *J. Immunol.* 179, 6808–6819.  
812 10.4049/jimmunol.179.10.6808.
- 813 40. Tomayko, M.M., Anderson, S.M., Brayton, C.E., Sadanand, S., Steinel, N.C.,  
814 Behrens, T.W., and Shlomchik, M.J. (2008). Systematic comparison of gene  
815 expression between murine memory and naive B cells demonstrates that memory B  
816 cells have unique signaling capabilities. *J. Immunol.* 181, 27–38.  
817 10.4049/jimmunol.181.1.27.
- 818 41. Wong, R., Belk, J.A., Govero, J., Uhrlaub, J.L., Reinartz, D., Zhao, H., Errico, J.M.,  
819 D’Souza, L., Ripperger, T.J., Nikolich-Zugich, J., et al. (2020). Affinity-Restricted  
820 Memory B Cells Dominate Recall Responses to Heterologous Flaviviruses.  
821 *Immunity* 53, 1078-1094.e7. 10.1016/j.immuni.2020.09.001.
- 822 42. Mesin, L., Schiepers, A., Ersching, J., Barbulescu, A., Cavazzoni, C.B., Angelini, A.,  
823 Okada, T., Kurosaki, T., and Victora, G.D. (2020). Restricted clonality and limited  
824 germinal center reentry characterize memory B cell reactivation by boosting. *Cell*  
825 180, 92-106.e11. 10.1016/j.cell.2019.11.032.



- 826 43. Purtha, W.E., Tedder, T.F., Johnson, S., Bhattacharya, D., and Diamond, M.S.  
827 (2011). Memory B cells, but not long-lived plasma cells, possess antigen  
828 specificities for viral escape mutants. *J. Exp. Med.* *208*, 2599–2606.  
829 10.1084/jem.20110740.
- 830 44. Francis, T. (1960). On the Doctrine of Original Antigenic Sin. *Proc. Am. Philos. Soc.*  
831 *104*, 572–578.
- 832 45. Worobey, M., Plotkin, S., and Hensley, S.E. (2020). Influenza Vaccines Delivered in  
833 Early Childhood Could Turn Antigenic Sin into Antigenic Blessings. *Cold Spring*  
834 *Harb. Perspect. Med.* *10*. 10.1101/cshperspect.a038471.
- 835 46. Anderson, E.M., Li, S.H., Awofolaju, M., Eilola, T., Goodwin, E., Bolton, M.J.,  
836 Gouma, S., Manzoni, T.B., Hicks, P., Goel, R.R., et al. (2022). SARS-CoV-2  
837 infections elicit higher levels of original antigenic sin antibodies compared with  
838 SARS-CoV-2 mRNA vaccinations. *Cell Rep.* *41*, 111496.  
839 10.1016/j.celrep.2022.111496.
- 840 47. Amanat, F., Thapa, M., Lei, T., Sayed Ahmed, S.M., Adelsberg, D.C., Carreno,  
841 J.M., Strohmeier, S., Schmitz, A.J., Zafar, S., Zhou, J.Q., et al. (2021). SARS-CoV-  
842 2 mRNA vaccination induces functionally diverse antibodies to NTD, RBD and S2.  
843 *Cell.* 10.1016/j.cell.2021.06.005.
- 844 48. Worobey, M., Han, G.-Z., and Rambaut, A. (2014). Genesis and pathogenesis of  
845 the 1918 pandemic H1N1 influenza A virus. *Proc. Natl. Acad. Sci. U. S. A.* *111*,  
846 8107–8112. 10.1073/pnas.1324197111.

- 847 49. Taubenberger, J.K., and Morens, D.M. (2006). 1918 Influenza: the mother of all  
848 pandemics. *Emerg. Infect. Dis.* *12*, 15–22. [10.3201/eid1201.050979](https://doi.org/10.3201/eid1201.050979).
- 849 50. Gostic, K.M., Bridge, R., Brady, S., Viboud, C., Worobey, M., and Lloyd-Smith, J.O.  
850 (2019). Childhood immune imprinting to influenza A shapes birth year-specific risk  
851 during seasonal H1N1 and H3N2 epidemics. *PLoS Pathog.* *15*, e1008109.  
852 [10.1371/journal.ppat.1008109](https://doi.org/10.1371/journal.ppat.1008109).
- 853 51. Gostic, K.M., Ambrose, M., Worobey, M., and Lloyd-Smith, J.O. (2016). Potent  
854 protection against H5N1 and H7N9 influenza via childhood hemagglutinin  
855 imprinting. *Science* *354*, 722–726. [10.1126/science.aag1322](https://doi.org/10.1126/science.aag1322).
- 856 52. Greaney, A.J., Eguia, R.T., Starr, T.N., Khan, K., Franko, N., Logue, J.K., Lord,  
857 S.M., Speake, C., Chu, H.Y., Sigal, A., et al. (2022). The SARS-CoV-2 Delta variant  
858 induces an antibody response largely focused on class 1 and 2 antibody epitopes.  
859 *PLoS Pathog.* *18*, e1010592. [10.1371/journal.ppat.1010592](https://doi.org/10.1371/journal.ppat.1010592).
- 860 53. Abbott, R.K., Lee, J.H., Menis, S., Skog, P., Rossi, M., Ota, T., Kulp, D.W., Bhullar,  
861 D., Kalyuzhniy, O., Havenar-Daughton, C., et al. (2018). Precursor Frequency and  
862 Affinity Determine B Cell Competitive Fitness in Germinal Centers, Tested with  
863 Germline-Targeting HIV Vaccine Immunogens. *Immunity* *48*, 133-146.e6.  
864 [10.1016/j.immuni.2017.11.023](https://doi.org/10.1016/j.immuni.2017.11.023).
- 865 54. Chan, T.D., Gatto, D., Wood, K., Camidge, T., Basten, A., and Brink, R. (2009).  
866 Antigen affinity controls rapid T-dependent antibody production by driving the

- 867 expansion rather than the differentiation or extrafollicular migration of early  
868 plasmablasts. *J. Immunol.* *183*, 3139–3149. 10.4049/jimmunol.0901690.
- 869 55. Anderson, S.M., Khalil, A., Uduman, M., Hershberg, U., Louzoun, Y., Haberman,  
870 A.M., Kleinstein, S.H., and Shlomchik, M.J. (2009). Taking advantage: high-affinity  
871 B cells in the germinal center have lower death rates, but similar rates of division,  
872 compared to low-affinity cells. *J. Immunol.* *183*, 7314–7325.  
873 10.4049/jimmunol.0902452.
- 874 56. Shih, T.-A.Y., Meffre, E., Roederer, M., and Nussenzweig, M.C. (2002). Role of  
875 BCR affinity in T cell dependent antibody responses in vivo. *Nat. Immunol.* *3*, 570–  
876 575. 10.1038/ni803.
- 877 57. Yeh, C.-H., Nojima, T., Kuraoka, M., and Kelsoe, G. (2018). Germinal center entry  
878 not selection of B cells is controlled by peptide-MHCII complex density. *Nat.*  
879 *Commun.* *9*, 1–11. 10.1038/s41467-018-03382-x.
- 880 58. Kwong, P.D., Wyatt, R., Robinson, J., Sweet, R.W., Sodroski, J., and Hendrickson,  
881 W.A. (1998). Structure of an HIV gp120 envelope glycoprotein in complex with the  
882 CD4 receptor and a neutralizing human antibody. *Nature* *393*, 648–659.  
883 10.1038/31405.
- 884 59. Grant, O.C., Montgomery, D., Ito, K., and Woods, R.J. (2020). Analysis of the  
885 SARS-CoV-2 spike protein glycan shield reveals implications for immune  
886 recognition. *Sci. Rep.* *10*, 14991. 10.1038/s41598-020-71748-7.

- 887 60. Chan, T.D., Wood, K., Hermes, J.R., Butt, D., Jolly, C.J., Basten, A., and Brink, R.  
888 (2012). Elimination of germinal-center-derived self-reactive B cells is governed by  
889 the location and concentration of self-antigen. *Immunity* 37, 893–904.  
890 10.1016/j.immuni.2012.07.017.
- 891 61. Reed, J.H., Jackson, J., Christ, D., and Goodnow, C.C. (2016). Clonal redemption  
892 of autoantibodies by somatic hypermutation away from self-reactivity during human  
893 immunization. *J. Exp. Med.* 213, 1255–1265. 10.1084/jem.20151978.
- 894 62. Sabouri, Z., Schofield, P., Horikawa, K., Spierings, E., Kipling, D., Randall, K.L.,  
895 Langley, D., Roome, B., Vazquez-Lombardi, R., Rouet, R., et al. (2014).  
896 Redemption of autoantibodies on anergic B cells by variable-region glycosylation  
897 and mutation away from self-reactivity. *Proc. Natl. Acad. Sci. U. S. A.* 111, E2567-  
898 75. 10.1073/pnas.1406974111.
- 899 63. Sangesland, M., Torrents de la Peña, A., Boyoglu-Barnum, S., Ronsard, L.,  
900 Mohamed, F.A.N., Moreno, T.B., Barnes, R.M., Rohrer, D., Lonberg, N.,  
901 Ghebremichael, M., et al. (2022). Allelic polymorphism controls autoreactivity and  
902 vaccine elicitation of human broadly neutralizing antibodies against influenza virus.  
903 *Immunity* 55, 1693-1709.e8. 10.1016/j.immuni.2022.07.006.
- 904 64. Berman, J.E., Nickerson, K.G., Pollock, R.R., Barth, J.E., Schuurman, R.K.,  
905 Knowles, D.M., Chess, L., and Alt, F.W. (1991). VH gene usage in humans: biased  
906 usage of the VH6 gene in immature B lymphoid cells. *Eur. J. Immunol.* 21, 1311–  
907 1314. 10.1002/eji.1830210532.

- 908 65. Willems van Dijk, K., Milner, L.A., Sasso, E.H., and Milner, E.C. (1992).  
909 Chromosomal organization of the heavy chain variable region gene segments  
910 comprising the human fetal antibody repertoire. *Proc. Natl. Acad. Sci. U. S. A.* *89*,  
911 10430–10434. [10.1073/pnas.89.21.10430](https://doi.org/10.1073/pnas.89.21.10430).
- 912 66. Nadel, B., Tang, A., Lugo, G., Love, V., Escuro, G., and Feeney, A.J. (1998).  
913 Decreased frequency of rearrangement due to the synergistic effect of nucleotide  
914 changes in the heptamer and nonamer of the recombination signal sequence of the  
915 V kappa gene A2b, which is associated with increased susceptibility of Navajos to  
916 Haemophilus influenzae type b disease. *J. Immunol.* *161*, 6068–6073.
- 917 67. Murray, S.M., Ansari, A.M., Frater, J., Klenerman, P., Dunachie, S., Barnes, E., and  
918 Ogbe, A. (2023). The impact of pre-existing cross-reactive immunity on SARS-CoV-  
919 2 infection and vaccine responses. *Nat. Rev. Immunol.* *23*, 304–316.  
920 [10.1038/s41577-022-00809-x](https://doi.org/10.1038/s41577-022-00809-x).
- 921 68. Chemaitelly, H., Ayoub, H.H., Tang, P., Hasan, M.R., Coyle, P., Yassine, H.M., Al-  
922 Khatib, H.A., Smatti, M.K., Al-Kanaani, Z., Al-Kuwari, E., et al. (2022). Immune  
923 Imprinting and Protection against Repeat Reinfection with SARS-CoV-2. *N. Engl. J.*  
924 *Med.* [10.1056/NEJMc2211055](https://doi.org/10.1056/NEJMc2211055).
- 925 69. Koutsakos, M., and Ellebedy, A.H. (2023). Immunological imprinting: Understanding  
926 COVID-19. *Immunity* *56*, 909–913. [10.1016/j.immuni.2023.04.012](https://doi.org/10.1016/j.immuni.2023.04.012).
- 927 70. Alsoussi, W.B., Malladi, S.K., Zhou, J.Q., Liu, Z., Ying, B., Kim, W., Schmitz, A.J.,  
928 Lei, T., Horvath, S.C., Sturtz, A.J., et al. (2023). SARS-CoV-2 Omicron boosting

- 929 induces de novo B cell response in humans. *Nature* 617, 592–598.  
930 10.1038/s41586-023-06025-4.
- 931 71. Cao, Y., Yisimayi, A., Jian, F., Song, W., Xiao, T., Wang, L., Du, S., Wang, J., Li,  
932 Q., Chen, X., et al. (2022). BA.2.12.1, BA.4 and BA.5 escape antibodies elicited by  
933 Omicron infection. *Nature* 608, 593–602. 10.1038/s41586-022-04980-y.
- 934 72. Cao, Y., Jian, F., Wang, J., Yu, Y., Song, W., Yisimayi, A., Wang, J., An, R., Chen,  
935 X., Zhang, N., et al. (2023). Imprinted SARS-CoV-2 humoral immunity induces  
936 convergent Omicron RBD evolution. *Nature* 614, 521–529. 10.1038/s41586-022-  
937 05644-7.
- 938 73. Park, Y.-J., Pinto, D., Walls, A.C., Liu, Z., De Marco, A., Benigni, F., Zatta, F.,  
939 Silacci-Fregni, C., Bassi, J., Sprouse, K.R., et al. (2022). Imprinted antibody  
940 responses against SARS-CoV-2 Omicron sublineages. *Science* 378, 619–627.  
941 10.1126/science.adc9127.
- 942 74. Reynolds, C.J., Gibbons, J.M., Pade, C., Lin, K.-M., Sandoval, D.M., Pieper, F.,  
943 Butler, D.K., Liu, S., Otter, A.D., Joy, G., et al. (2022). Heterologous infection and  
944 vaccination shapes immunity against SARS-CoV-2 variants. *Science* 375, 183–192.  
945 10.1126/science.abm0811.
- 946 75. Gagne, M., Moliva, J.I., Foulds, K.E., Andrew, S.F., Flynn, B.J., Werner, A.P.,  
947 Wagner, D.A., Teng, I.-T., Lin, B.C., Moore, C., et al. (2022). mRNA-1273 or  
948 mRNA-Omicron boost in vaccinated macaques elicits similar B cell expansion,

- 949 neutralizing responses, and protection from Omicron. *Cell* 185, 1556-1571.e18.  
950 10.1016/j.cell.2022.03.038.
- 951 76. Masurel, N. (1969). RELATION BETWEEN HONG KONG VIRUS AND FORMER  
952 HUMAN A2 ISOLATES AND THE A/EQUI2 VIRUS IN HUMAN SERA COLLECTED  
953 BEFORE 1957. *Lancet* 293, 907–910. 10.1016/S0140-6736(69)92544-6.
- 954 77. Masurel, N., and Heijntink, R.A. (1983). Recycling of H1N1 influenza A virus in man--  
955 a haemagglutinin antibody study. *J. Hyg.* 90, 397–402.  
956 10.1017/s0022172400029028.
- 957 78. Akinbami, L.J., Kruszon-Moran, D., Wang, C.-Y., Storandt, R.J., Clark, J., Riddles,  
958 M.K., and Mohadjer, L.K. (2022). SARS-CoV-2 serology and self-reported infection  
959 among adults - National Health and Nutrition Examination Survey, United States,  
960 august 2021-may 2022. *MMWR Morb. Mortal. Wkly. Rep.* 71, 1522–1525.  
961 10.15585/mmwr.mm7148a4.
- 962 79. Zhang, Z., Mateus, J., Coelho, C.H., Dan, J.M., Moderbacher, C.R., Gálvez, R.I.,  
963 Cortes, F.H., Grifoni, A., Tarke, A., Chang, J., et al. (2022). Humoral and cellular  
964 immune memory to four COVID-19 vaccines. *Cell* 185, 2434-2451.e17.  
965 10.1016/j.cell.2022.05.022.
- 966 80. Jones, J.M., Manrique, I.M., Stone, M.S., Grebe, E., Saa, P., Germanio, C.D.,  
967 Spencer, B.R., Notari, E., Bravo, M., Lanteri, M.C., et al. (2023). Estimates of  
968 SARS-CoV-2 seroprevalence and incidence of primary SARS-CoV-2 infections  
969 among blood donors, by COVID-19 vaccination status - United States, April 2021-

- 970        September 2022. *MMWR Morb. Mortal. Wkly. Rep.* 72, 601–605.
- 971        10.15585/mmwr.mm7222a3.
- 972    81. Kaplonek, P., Fischinger, S., Cizmeci, D., Bartsch, Y.C., Kang, J., Burke, J.S., Shin,  
973        S.A., Dayal, D., Martin, P., Mann, C., et al. (2022). mRNA-1273 vaccine-induced  
974        antibodies maintain Fc-effector functions across SARS-CoV-2 Variants of Concern.  
975        *Immunity*. 10.1016/j.immuni.2022.01.001.
- 976    82. Lutrick, K., Ellingson, K.D., Baccam, Z., Rivers, P., Beitel, S., Parker, J., Hollister,  
977        J., Sun, X., Gerald, J.K., Komatsu, K., et al. (2021). COVID-19 infection, reinfection,  
978        and vaccine effectiveness in a prospective cohort of Arizona frontline/essential  
979        workers: The AZ HEROES research protocol. *JMIR Res. Protoc.* 10, e28925.  
980        10.2196/28925.
- 981    83. Goel, R.R., Apostolidis, S.A., Painter, M.M., Mathew, D., Pattekar, A., Kuthuru, O.,  
982        Gouma, S., Hicks, P., Meng, W., Rosenfeld, A.M., et al. (2021). Distinct antibody  
983        and memory B cell responses in SARS-CoV-2 naïve and recovered individuals  
984        following mRNA vaccination. *Sci Immunol* 6. 10.1126/sciimmunol.abi6950.
- 985    84. Edwards, L.J., Fowlkes, A.L., Wesley, M.G., Kuntz, J.L., Odean, M.J., Caban-  
986        Martinez, A.J., Dunnigan, K., Phillips, A.L., Grant, L., Herring, M.K., et al. (2021).  
987        “Research on the Epidemiology of SARS-CoV-2 in Essential Response Personnel  
988        (RECOVER) Study: Protocol for a multi-site longitudinal cohort.” *JMIR Res Protoc*  
989        7.



- 990 85. Greaney, A.J., Loes, A.N., Gentles, L.E., Crawford, K.H.D., Starr, T.N., Malone,  
991 K.D., Chu, H.Y., and Bloom, J.D. (2021). Antibodies elicited by mRNA-1273  
992 vaccination bind more broadly to the receptor binding domain than do those from  
993 SARS-CoV-2 infection. *Science Translational Medicine*.  
994 10.1126/scitranslmed.abi9915.
- 995 86. Rambaut, A., Holmes, E.C., O’Toole, Á., Hill, V., McCrone, J.T., Ruis, C., du  
996 Plessis, L., and Pybus, O.G. (2020). A dynamic nomenclature proposal for SARS-  
997 CoV-2 lineages to assist genomic epidemiology. *Nat. Microbiol.* 5, 1403–1407.  
998 10.1038/s41564-020-0770-5.
- 999 87. Cherian, S., Potdar, V., Jadhav, S., Yadav, P., Gupta, N., Das, M., Rakshit, P.,  
1000 Singh, S., Abraham, P., Panda, S., et al. (2021). SARS-CoV-2 spike mutations,  
1001 L452R, T478K, E484Q and P681R, in the second wave of COVID-19 in  
1002 Maharashtra, India. *Microorganisms* 9, 1542. 10.3390/microorganisms9071542.
- 1003 88. Ripperger, T.J., Uhrlaub, J.L., Watanabe, M., Wong, R., Castaneda, Y., Pizzato,  
1004 H.A., Thompson, M.R., Bradshaw, C., Weinkauff, C.C., Bime, C., et al. (2020).  
1005 Orthogonal SARS-CoV-2 Serological Assays Enable Surveillance of Low-  
1006 Prevalence Communities and Reveal Durable Humoral Immunity. *Immunity* 53,  
1007 925-933.e4. 10.1016/j.immuni.2020.10.004.
- 1008 89. Piccoli, L., Park, Y.-J., Tortorici, M.A., Czudnochowski, N., Walls, A.C., Beltramello,  
1009 M., Silacci-Fregni, C., Pinto, D., Rosen, L.E., Bowen, J.E., et al. (2020). Mapping  
1010 Neutralizing and Immunodominant Sites on the SARS-CoV-2 Spike Receptor-

- 1011 Binding Domain by Structure-Guided High-Resolution Serology. *Cell* **183**, 1024-  
1012 1042.e21. [10.1016/j.cell.2020.09.037](https://doi.org/10.1016/j.cell.2020.09.037).
- 1013 90. Greaney, A.J., Loes, A.N., Crawford, K.H.D., Starr, T.N., Malone, K.D., Chu, H.Y.,  
1014 and Bloom, J.D. (2021). Comprehensive mapping of mutations in the SARS-CoV-2  
1015 receptor-binding domain that affect recognition by polyclonal human plasma  
1016 antibodies. *Cell Host Microbe* **29**, 463-476.e6. [10.1016/j.chom.2021.02.003](https://doi.org/10.1016/j.chom.2021.02.003).
- 1017 91. Röltgen, K., Nielsen, S.C.A., Silva, O., Younes, S.F., Zaslavsky, M., Costales, C.,  
1018 Yang, F., Wirz, O.F., Solis, D., Hoh, R.A., et al. (2022). Immune imprinting, breadth  
1019 of variant recognition, and germinal center response in human SARS-CoV-2  
1020 infection and vaccination. *Cell* **185**, 1025-1040.e14. [10.1016/j.cell.2022.01.018](https://doi.org/10.1016/j.cell.2022.01.018).
- 1021 92. Suryadevara, N., Shrihari, S., Gilchuk, P., VanBlargan, L.A., Binshtein, E., Zost,  
1022 S.J., Nargi, R.S., Sutton, R.E., Winkler, E.S., Chen, E.C., et al. (2021). Neutralizing  
1023 and protective human monoclonal antibodies recognizing the N-terminal domain of  
1024 the SARS-CoV-2 spike protein. *Cell* **184**, 2316-2331.e15.  
1025 [10.1016/j.cell.2021.03.029](https://doi.org/10.1016/j.cell.2021.03.029).
- 1026 93. Cerutti, G., Guo, Y., Zhou, T., Gorman, J., Lee, M., Rapp, M., Reddem, E.R., Yu, J.,  
1027 Bahna, F., Bimela, J., et al. (2021). Potent SARS-CoV-2 neutralizing antibodies  
1028 directed against spike N-terminal domain target a single supersite. *Cell Host*  
1029 *Microbe* **29**, 819-833.e7. [10.1016/j.chom.2021.03.005](https://doi.org/10.1016/j.chom.2021.03.005).
- 1030 94. McCallum, M., De Marco, A., Lempp, F.A., Tortorici, M.A., Pinto, D., Walls, A.C.,  
1031 Beltramello, M., Chen, A., Liu, Z., Zatta, F., et al. (2021). N-terminal domain

- 1032 antigenic mapping reveals a site of vulnerability for SARS-CoV-2. *Cell* **184**, 2332-  
1033 2347.e16. [10.1016/j.cell.2021.03.028](https://doi.org/10.1016/j.cell.2021.03.028).
- 1034 95. Shroff, R.T., Chalasani, P., Wei, R., Pennington, D., Quirk, G., Schoenle, M.V.,  
1035 Peyton, K.L., Uhrlaub, J.L., Ripperger, T.J., Jergović, M., et al. (2021). Immune  
1036 responses to two and three doses of the BNT162b2 mRNA vaccine in adults with  
1037 solid tumors. *Nat. Med.*, 1–10. [10.1038/s41591-021-01542-z](https://doi.org/10.1038/s41591-021-01542-z).
- 1038 96. Motozono, C., Toyoda, M., Zahradnik, J., Saito, A., Nasser, H., Tan, T.S., Ngare, I.,  
1039 Kimura, I., Uriu, K., Kosugi, Y., et al. (2021). SARS-CoV-2 spike L452R variant  
1040 evades cellular immunity and increases infectivity. *Cell Host Microbe*.  
1041 [10.1016/j.chom.2021.06.006](https://doi.org/10.1016/j.chom.2021.06.006).
- 1042 97. He, P., Liu, B., Gao, X., Yan, Q., Pei, R., Sun, J., Chen, Q., Hou, R., Li, Z., Zhang,  
1043 Y., et al. (2022). SARS-CoV-2 Delta and Omicron variants evade population  
1044 antibody response by mutations in a single spike epitope. *Nat Microbiol*.  
1045 [10.1038/s41564-022-01235-4](https://doi.org/10.1038/s41564-022-01235-4).
- 1046 98. Tchesnokova, V., Kulasekara, H., Larson, L., Bowers, V., Rechkina, E., Kisiela, D.,  
1047 Sledneva, Y., Choudhury, D., Maslova, I., Deng, K., et al. (2021). Acquisition of the  
1048 L452R mutation in the ACE2-binding interface of spike protein triggers recent  
1049 massive expansion of SARS-CoV-2 variants. *J. Clin. Microbiol.* **59**, e0092121.  
1050 [10.1128/JCM.00921-21](https://doi.org/10.1128/JCM.00921-21).
- 1051 99. Greaney, A.J., Starr, T.N., Eguia, R.T., Loes, A.N., Khan, K., Karim, F., Cele, S.,  
1052 Bowen, J.E., Logue, J.K., Corti, D., et al. (2022). A SARS-CoV-2 variant elicits an

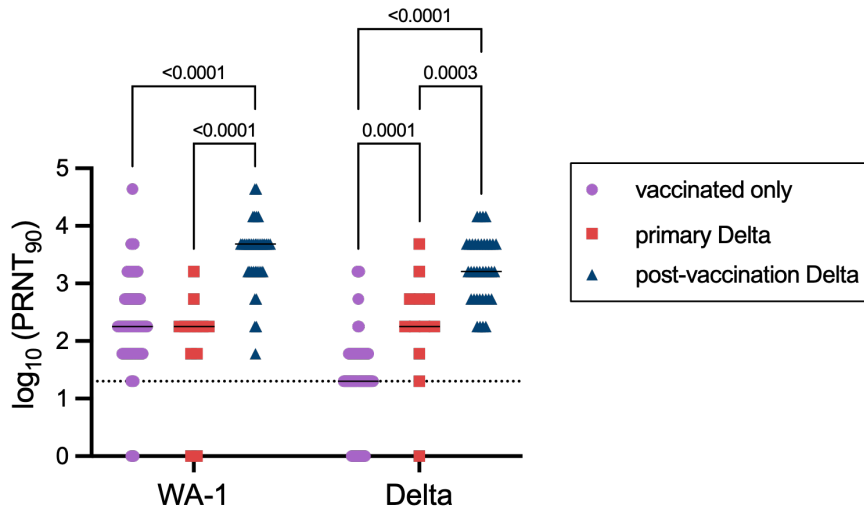
- 1053 antibody response with a shifted immunodominance hierarchy. *PLoS Pathog.* *18*,  
1054 e1010248. [10.1371/journal.ppat.1010248](https://doi.org/10.1371/journal.ppat.1010248).
- 1055 100. Setliff, I., Shiakolas, A.R., Pilewski, K.A., Murji, A.A., Mapengo, R.E., Janowska,  
1056 K., Richardson, S., Oosthuysen, C., Raju, N., Ronsard, L., et al. (2019). High-  
1057 Throughput Mapping of B Cell Receptor Sequences to Antigen Specificity. *Cell* *179*,  
1058 1636-1646.e15. [10.1016/j.cell.2019.11.003](https://doi.org/10.1016/j.cell.2019.11.003).
- 1059 101. Schiepers, A., van 't Wout, M.F.L., Greaney, A.J., Zang, T., Muramatsu, H., Lin,  
1060 P.J.C., Tam, Y.K., Mesin, L., Starr, T.N., Bieniasz, P.D., et al. (2023). Molecular  
1061 fate-mapping of serum antibody responses to repeat immunization. *Nature*.  
1062 [10.1038/s41586-023-05715-3](https://doi.org/10.1038/s41586-023-05715-3).
- 1063 102. Horwitz, L.I., Thaweethai, T., Brosnahan, S.B., Cicek, M.S., Fitzgerald, M.L.,  
1064 Goldman, J.D., Hess, R., Hodder, S.L., Jacoby, V.L., Jordan, M.R., et al. (2023).  
1065 Researching COVID to Enhance Recovery (RECOVER) adult study protocol:  
1066 Rationale, objectives, and design. *PLoS One* *18*, e0286297.  
1067 [10.1371/journal.pone.0286297](https://doi.org/10.1371/journal.pone.0286297).
- 1068 103. Smith, K.G., Light, A., Nossal, G.J., and Tarlinton, D.M. (1997). The extent of  
1069 affinity maturation differs between the memory and antibody-forming cell  
1070 compartments in the primary immune response. *EMBO J.* *16*, 2996–3006.  
1071 [10.1093/emboj/16.11.2996](https://doi.org/10.1093/emboj/16.11.2996).
- 1072 104. Lavinder, J.J., Wine, Y., Giesecke, C., Ippolito, G.C., Horton, A.P., Lungu, O.I.,  
1073 Hoi, K.H., DeKosky, B.J., Murrin, E.M., Wirth, M.M., et al. (2014). Identification and

- 1074 characterization of the constituent human serum antibodies elicited by vaccination.  
1075 Proc. Natl. Acad. Sci. U. S. A. *111*, 2259–2264. 10.1073/pnas.1317793111.
- 1076 105. Pape, K.A., Maul, R.W., Dileepan, T., Paustian, A.S., Gearhart, P.J., and  
1077 Jenkins, M.K. (2018). Naive B cells with high-avidity germline-encoded antigen  
1078 receptors produce persistent IgM+ and transient IgG+ memory B cells. *Immunity* *48*,  
1079 1135-1143.e4. 10.1016/j.immuni.2018.04.019.
- 1080 106. Andrews, S.F., Kaur, K., Pauli, N.T., Huang, M., Huang, Y., and Wilson, P.C.  
1081 (2015). High preexisting serological antibody levels correlate with diversification of  
1082 the influenza vaccine response. *J. Virol.* *89*, 3308–3317. 10.1128/JVI.02871-14.
- 1083 107. Inoue, T., Shinnakasu, R., Kawai, C., Yamamoto, H., Sakakibara, S., Ono, C.,  
1084 Itoh, Y., Terooatea, T., Yamashita, K., Okamoto, T., et al. (2023). Antibody  
1085 feedback contributes to facilitating the development of Omicron-reactive memory B  
1086 cells in SARS-CoV-2 mRNA vaccinees. *J. Exp. Med.* *220*. 10.1084/jem.20221786.
- 1087 108. Liu, Y.J., Zhang, J., Lane, P.J., Chan, E.Y., and MacLennan, I.C. (1991). Sites of  
1088 specific B cell activation in primary and secondary responses to T cell-dependent  
1089 and T cell-independent antigens. *Eur. J. Immunol.* *21*, 2951–2962.  
1090 10.1002/eji.1830211209.
- 1091 109. Abbott, R.K., and Crotty, S. (2020). Factors in B cell competition and  
1092 immunodominance. *Immunol. Rev.* *296*, 120–131. 10.1111/imr.12861.
- 1093 110. Krammer, F. (2019). The human antibody response to influenza A virus infection  
1094 and vaccination. *Nat. Rev. Immunol.* *19*, 383–397. 10.1038/s41577-019-0143-6.

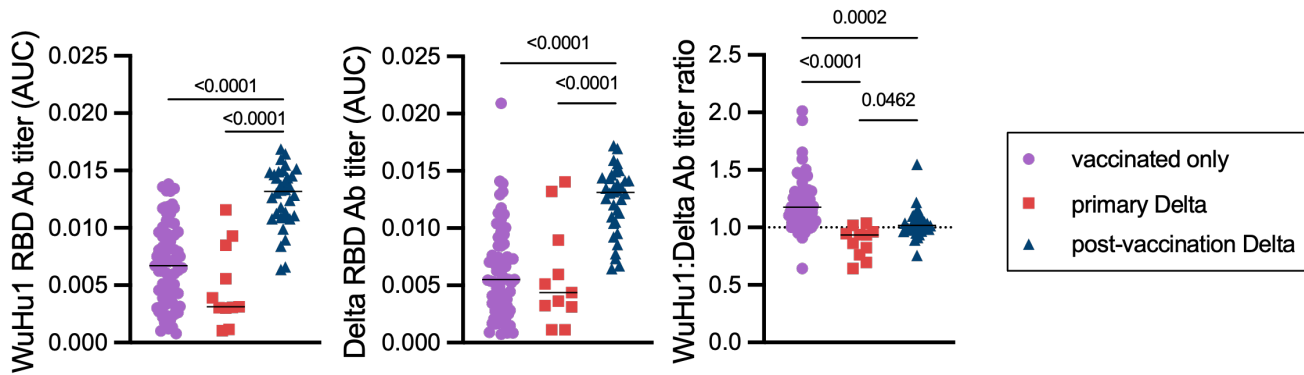
- 1095 111. Chia, P.Y., Ong, S.W.X., Chiew, C.J., Ang, L.W., Chavatte, J.-M., Mak, T.-M.,  
1096 Cui, L., Kalimuddin, S., Chia, W.N., Tan, C.W., et al. (2022). Virological and  
1097 serological kinetics of SARS-CoV-2 Delta variant vaccine breakthrough infections: a  
1098 multicentre cohort study. *Clin. Microbiol. Infect.* 28, 612.e1-612.e7.  
1099 10.1016/j.cmi.2021.11.010.
- 1100 112. Schaefer-Babajew, D., Wang, Z., Muecksch, F., Cho, A., Loewe, M., Cipolla, M.,  
1101 Raspe, R., Johnson, B., Canis, M., DaSilva, J., et al. (2023). Antibody feedback  
1102 regulates immune memory after SARS-CoV-2 mRNA vaccination. *Nature* 613, 735–  
1103 742. 10.1038/s41586-022-05609-w.
- 1104 113. Gao, Y., Cai, C., Grifoni, A., Müller, T.R., Niessl, J., Olofsson, A., Humbert, M.,  
1105 Hansson, L., Österborg, A., Bergman, P., et al. (2022). Ancestral SARS-CoV-2-  
1106 specific T cells cross-recognize the Omicron variant. *Nat. Med.* 28, 472–476.  
1107 10.1038/s41591-022-01700-x.
- 1108 114. Keeton, R., Tincho, M.B., Ngomti, A., Baguma, R., Benede, N., Suzuki, A., Khan,  
1109 K., Cele, S., Bernstein, M., Karim, F., et al. (2022). T cell responses to SARS-CoV-2  
1110 spike cross-recognize Omicron. *Nature* 603, 488–492. 10.1038/s41586-022-04460-  
1111 3.
- 1112 115. Bartsch, Y.C., Wang, C., Zohar, T., Fischinger, S., Atyeo, C., Burke, J.S., Kang,  
1113 J., Edlow, A.G., Fasano, A., Baden, L.R., et al. (2021). Humoral signatures of  
1114 protective and pathological SARS-CoV-2 infection in children. *Nat. Med.* 27, 454–  
1115 462. 10.1038/s41591-021-01263-3.

- 1116 116. Ying, B., Scheaffer, S.M., Whitener, B., Liang, C.-Y., Dmytrenko, O., Mackin, S.,  
1117 Wu, K., Lee, D., Avena, L.E., Chong, Z., et al. (2022). Boosting with Omicron-  
1118 matched or historical mRNA vaccines increases neutralizing antibody responses  
1119 and protection against B.1.1.529 infection in mice. *bioRxiv*org, 2022.02.07.479419.  
1120 10.1101/2022.02.07.479419.
- 1121 117. Barnes, C.O., West, A.P., Jr, Huey-Tubman, K.E., Hoffmann, M.A.G., Sharaf,  
1122 N.G., Hoffman, P.R., Koranda, N., Gristick, H.B., Gaebler, C., Muecksch, F., et al.  
1123 (2020). Structures of Human Antibodies Bound to SARS-CoV-2 Spike Reveal  
1124 Common Epitopes and Recurrent Features of Antibodies. *Cell* 182, 828-842.e16.  
1125 10.1016/j.cell.2020.06.025.
- 1126 118. Hay, J.A., Kissler, S.M., Fauver, J.R., Mack, C., Tai, C.G., Samant, R.M.,  
1127 Connolly, S., Anderson, D.J., Khullar, G., MacKay, M., et al. (2022). Quantifying the  
1128 impact of immune history and variant on SARS-CoV-2 viral kinetics and infection  
1129 rebound: A retrospective cohort study. *Elife* 11. 10.7554/eLife.81849.
- 1130 119. Goldfarb, D.M., Tilley, P., Al-Rawahi, G.N., Srigley, J.A., Ford, G., Pedersen, H.,  
1131 Pabbi, A., Hannam-Clark, S., Charles, M., Dittrick, M., et al. (2020). Self-collected  
1132 saline gargle samples as an alternative to healthcare worker collected  
1133 nasopharyngeal swabs for COVID-19 diagnosis in outpatients. *J. Clin. Microbiol.*,  
1134 2020.09.13.20188334. 10.1101/2020.09.13.20188334.
- 1135 120. Hao, Y., Hao, S., Andersen-Nissen, E., Mauck, W.M., 3rd, Zheng, S., Butler, A.,  
1136 Lee, M.J., Wilk, A.J., Darby, C., Zager, M., et al. (2021). Integrated analysis of  
1137 multimodal single-cell data. *Cell* 184, 3573-3587.e29. 10.1016/j.cell.2021.04.048.

A.



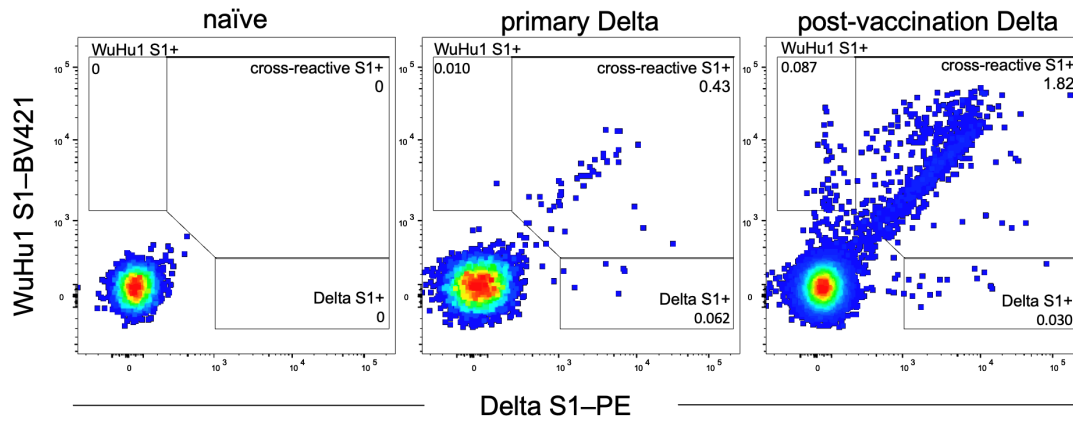
B.



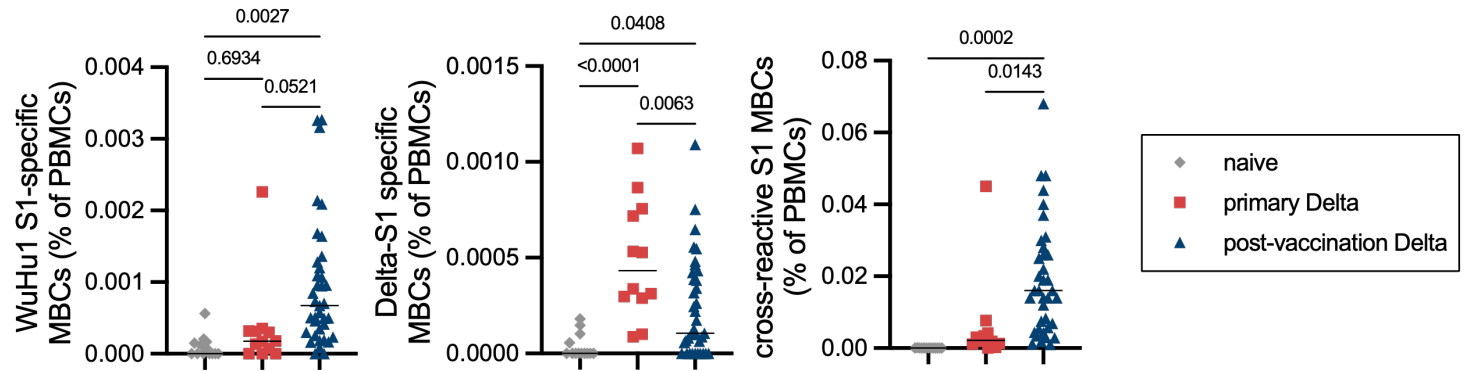


1138 **Figure 1. Primary and recall antibody responses to Wuhan and Delta strains of**  
1139 **SARS-COV-2. (A)** Virus neutralization assays were performed using the WA-1 and  
1140 Delta isolates of SARS-CoV-2. Serial 1:3 dilutions of serums were performed and tested  
1141 for the ability to prevent plaque formation on Vero cells. The lowest concentration  
1142 capable of preventing more than 90% of plaques was considered to be the PRNT<sub>90</sub>  
1143 value. Each symbol represents an individual. Two-sided P values from t-test statistics  
1144 were calculated for pairwise differences using two-way ANOVA. Post hoc testing for  
1145 multiple comparisons between draws was performed using Tukey's multiple  
1146 comparisons test. P values greater than 0.05 are not depicted. **(B)** Quantitative titers of  
1147 WuHu1- and Delta RBD-specific antibodies. Serum was initially diluted 1:60, serially  
1148 diluted 1:3, assessed by ELISA for binding to the listed antigens, and area under the  
1149 curve (AUC) values were calculated. Each symbol represents an individual. WuHu1  
1150 AUC values were divided by their Delta AUC titer in the same individual to calculate a  
1151 WuHu1:Delta RBD ratio in the rightmost panel. Two-sided P values from t-test statistics  
1152 were calculated for pairwise differences using one-way ANOVA. Post hoc testing for  
1153 multiple comparisons between draws was performed using Tukey's multiple  
1154 comparisons test. P values greater than 0.05 are not depicted.  
1155  
1156

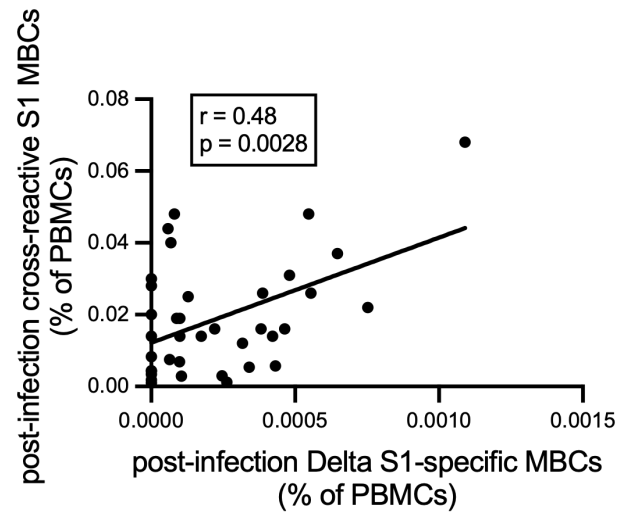
A.



B.

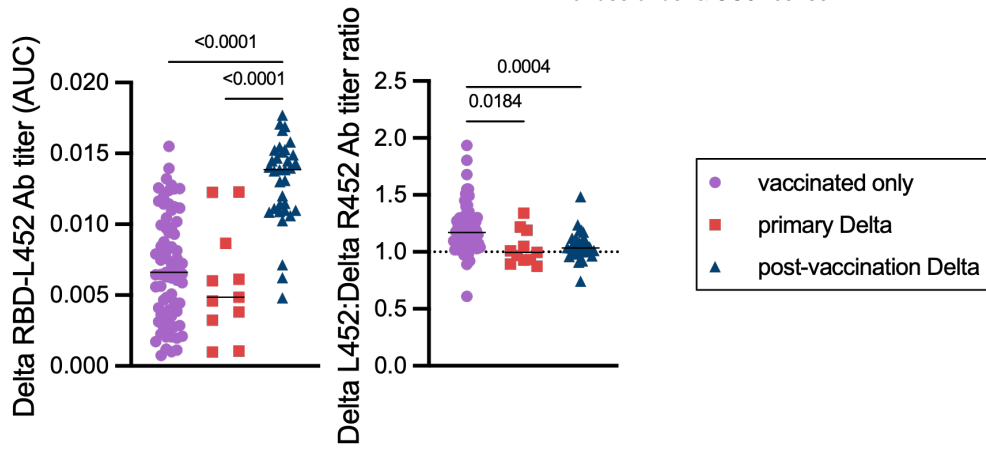


C.

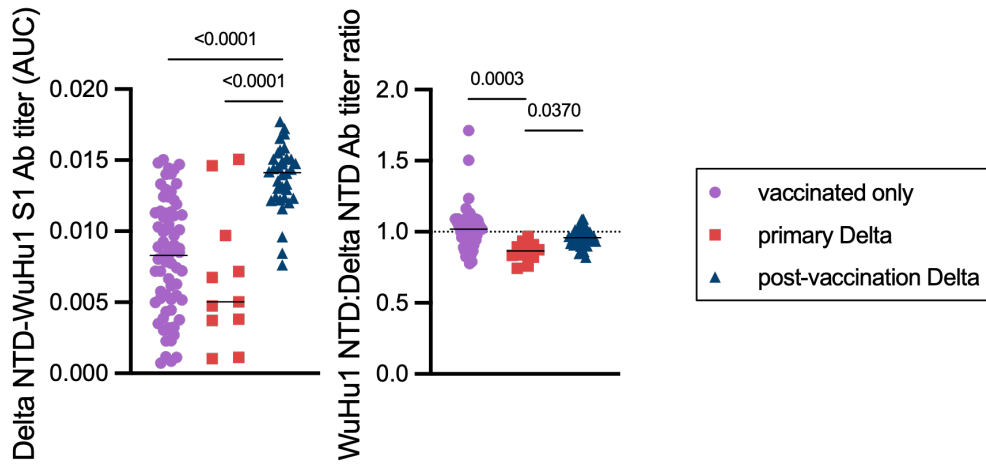


1157 **Figure 2. WuHu1 and Delta Memory B cell flow cytometric analysis and**  
1158 **quantification. (A)** Representative flow cytometric plots of Wuhu1 and Delta S1-  
1159 specific memory B cells (full gating strategy shown in Figure S2) in naïve, primary Delta  
1160 infection, and post-vaccination Delta infection cohorts. Cells that bind both WuHu1 S1  
1161 and Delta S1 are annotated as cross-reactive S1+, whereas cells that bind only WuHu1  
1162 S1 or Delta S1 are annotated as WuHu1 S1+ or Delta S1+, respectively. **(B)**  
1163 Quantification of isotype-switched memory B cells as a percentage of total PBMCs for  
1164 WuHu1 S1+, Delta S1+ and cross-reactive S1+ specificities for each cohort of SARS-  
1165 CoV-2 immune histories. Each symbol represents an individual. Two-sided P values  
1166 from t-test statistics were calculated for pairwise differences using one-way ANOVA.  
1167 Post hoc testing for multiple comparisons between draws was performed using Tukey's  
1168 multiple comparisons test. P values greater than 0.05 are not depicted. **(C)** Correlation  
1169 of post-infection cross-reactive S1 MBCs (calculated as in Figure 2B) plotted against the  
1170 frequency of post-infection Delta S1-specific MBCs (calculated as in Figure 2B) in  
1171 individuals that experienced a post-vaccination Delta infection. Pearson correlation  
1172 analysis was performed.  
1173  
1174

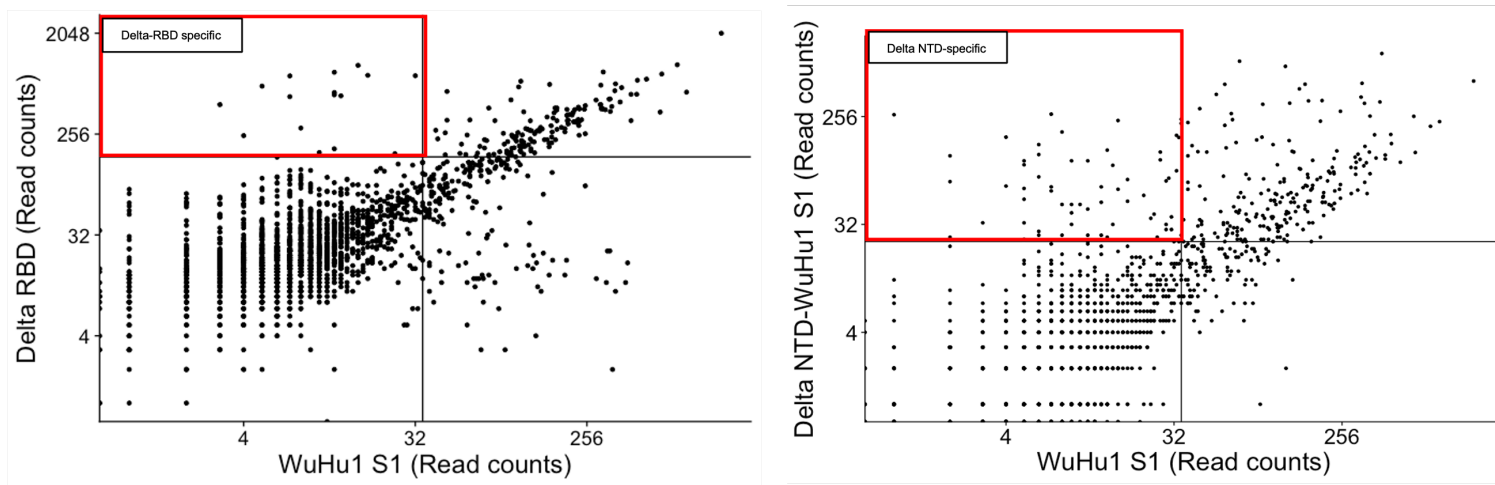
A.



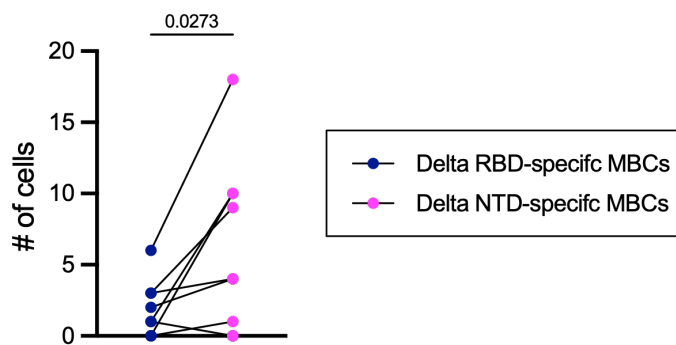
B.



C.



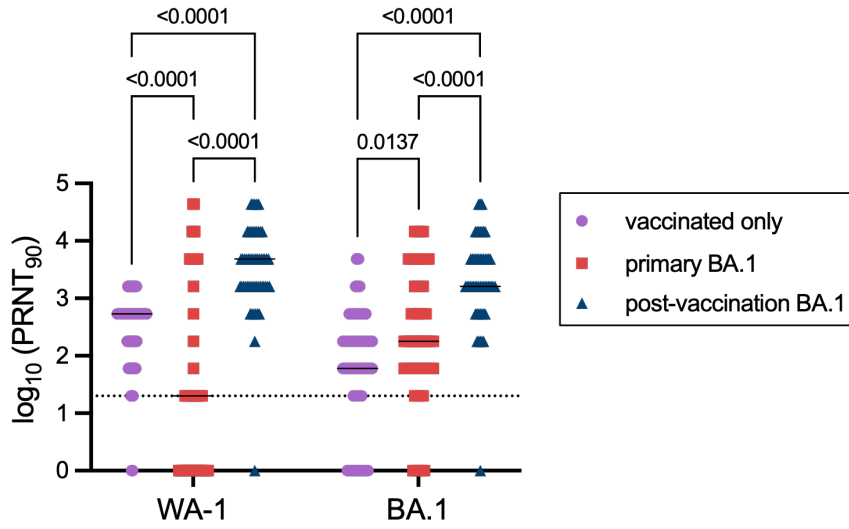
D.



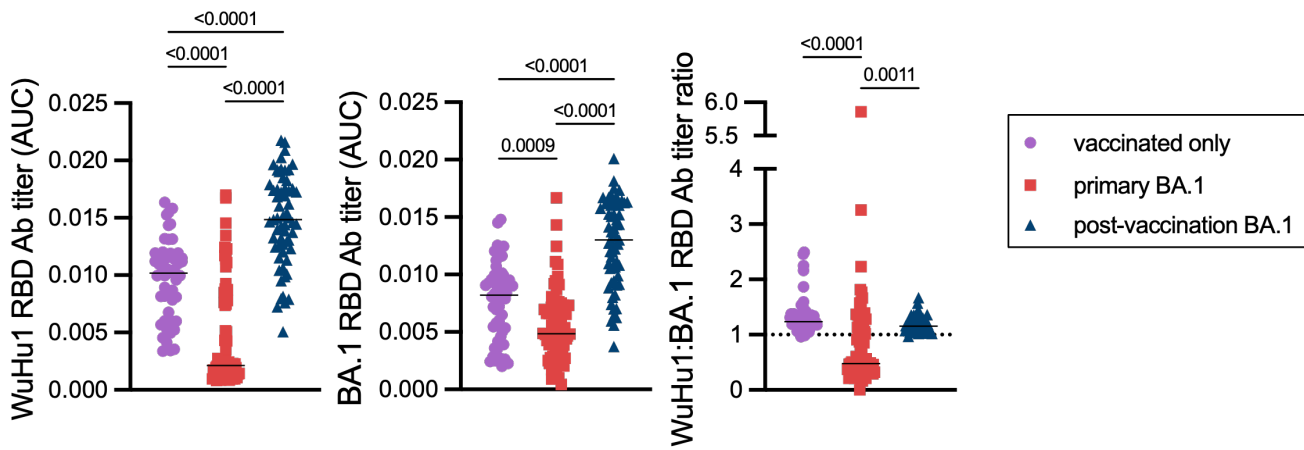
1175 **Figure 3. Epitope-specific quantification of Delta RBD- and Delta NTD-specific**  
1176 **antibodies and memory B cells. (A)** A chimeric protein (Delta RBD-L452) was  
1177 generated in which R452 was reverted to the ancestral L452. ELISAs were used to  
1178 quantify serum antibodies that bound to Delta RBD-L452 in each cohort. Delta RBD-  
1179 L452 AUC titers were divided by Delta RBD titers (Figure 1B) in the same individuals to  
1180 calculate a L452:R452 titer ratio. Each symbol represents an individual. Two-sided P  
1181 values from t-test statistics were calculated for pairwise differences using one-way  
1182 ANOVA. Post hoc testing for multiple comparisons between draws was performed using  
1183 Tukey's multiple comparisons test. P values greater than 0.05 are not depicted. **(B)** A  
1184 chimeric protein (Delta NTD-WuHu1 S1) was generated in which Delta NTD mutated  
1185 epitopes (T19R, G142D, E156-, F157-, R158G) were incorporated into the otherwise  
1186 WuHu1 S1 backbone. ELISAs were used to quantify serum antibodies that bound to  
1187 Delta NTD-WuHu1 S1 in each cohort. Delta RBD-L452 AUC titers were divided by their  
1188 Delta RBD (Supplemental Fig 1A) titer to calculate a WuHu1 NTD:Delta NTD titer ratio.  
1189 Each symbol represents an individual. Two-sided P values from t-test statistics were  
1190 calculated for pairwise differences using one-way ANOVA. Post hoc testing for multiple  
1191 comparisons between draws was performed using Tukey's multiple comparisons test. P  
1192 values greater than 0.05 are not depicted. **(C)** LIBRA-seq plots of isotype-switched  
1193 memory B cells enriched for Spike-binding specificities from primary Delta infections.  
1194 Read count thresholds to determine positivity were set using samples in which cells  
1195 lacking Spike-binding specificities were sorted and sequenced. Plots are concatenated  
1196 from ten individuals. **(D)** Quantification of Delta RBD-specific and Delta NTD-specific  
1197 memory B cells (MBCs) in individuals that experienced a primary Delta infection. Lines

1198 connect specificities within the same individual. Delta RBD-specific cells were classified  
1199 by cells that had Delta RBD read counts of greater than 160 and WuHu1 S1 read  
1200 counts of less than 35. Delta NTD-specific cells were classified by cells that had Delta  
1201 NTD-WuHu1 S1 read counts of greater than 23 and WuHu1 S1 read counts of less than  
1202 35. Two-sided P values were calculated for pairwise differences using paired t-tests.  
1203  
1204  
1205  
1206  
1207

A.



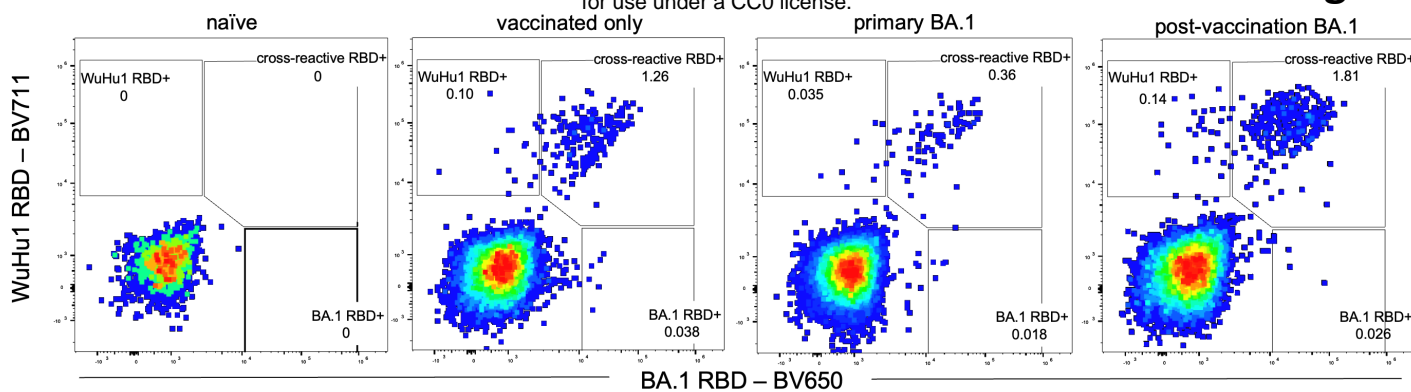
B.



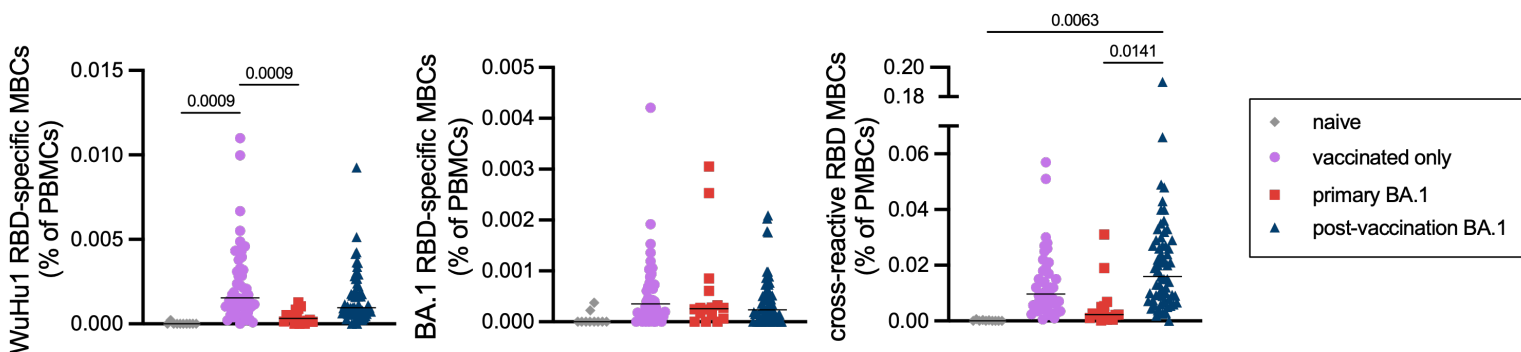
1208 **Figure 4. Primary and recall antibody responses to Wuhan and BA.1 strains of**  
1209 **SARS-COV-2. (A)** Virus neutralization assays were performed using the WA-1 and  
1210 BA.1 isolates of SARS-CoV-2. Serial 1:3 dilutions of serums were performed and tested  
1211 for the ability to prevent plaque formation on Vero cells. The lowest concentration  
1212 capable of preventing more than 90% of plaques was considered to the PRNT<sub>90</sub> value.  
1213 Each symbol represents an individual. Two-sided P values from t-test statistics were  
1214 calculated for pairwise differences using two-way ANOVA. Post hoc testing for multiple  
1215 comparisons between draws was performed using Tukey's multiple comparisons test. P  
1216 values greater than 0.05 are not depicted. **(B)** Quantitative titers of Wuhu1 and BA.1  
1217 RBD antibodies. Serum was initially diluted 1:60, serially diluted 1:3, assessed by  
1218 ELISA for binding to the listed antigens, and area under the curve (AUC) values were  
1219 calculated. Each symbol represents an individual. WuHu1 AUC values were divided by  
1220 their BA.1 RBD AUC titer in the same individual to calculate a ratio in the rightmost  
1221 panel. Two-sided P values from t-test statistics were calculated for pairwise differences  
1222 using one-way ANOVA. Post hoc testing for multiple comparisons between draws was  
1223 performed using Tukey's multiple comparisons test. P values greater than 0.05 are not  
1224 depicted.  
1225  
1226



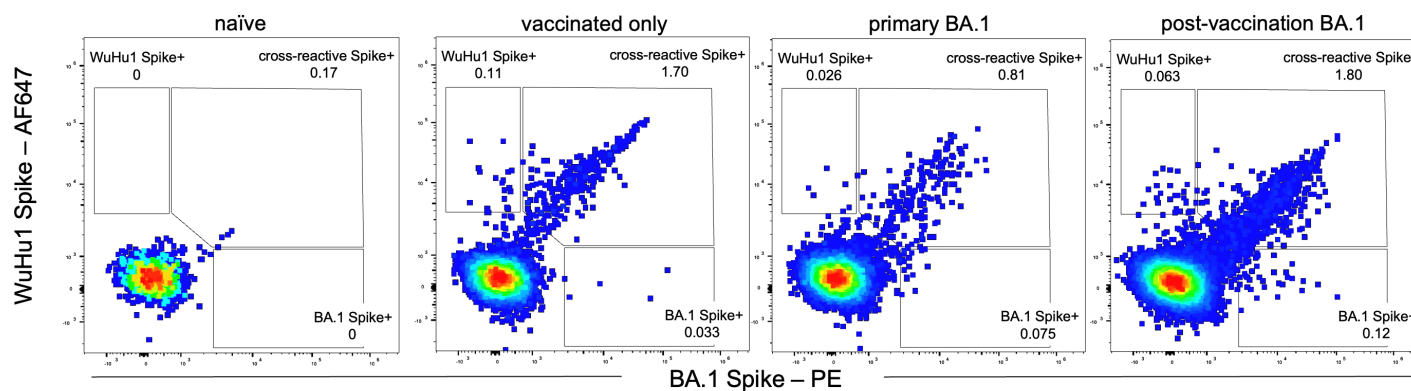
A.



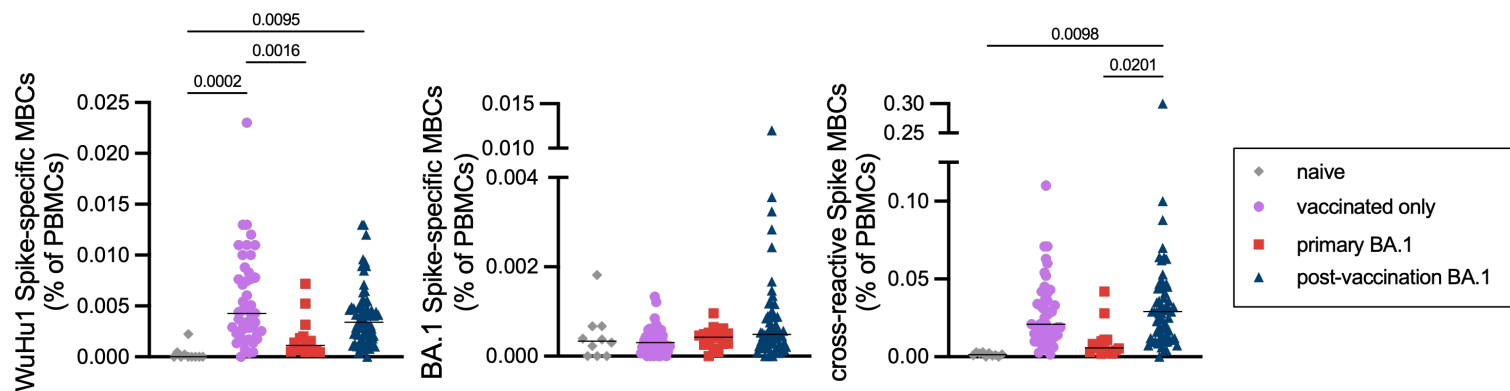
B.



C.

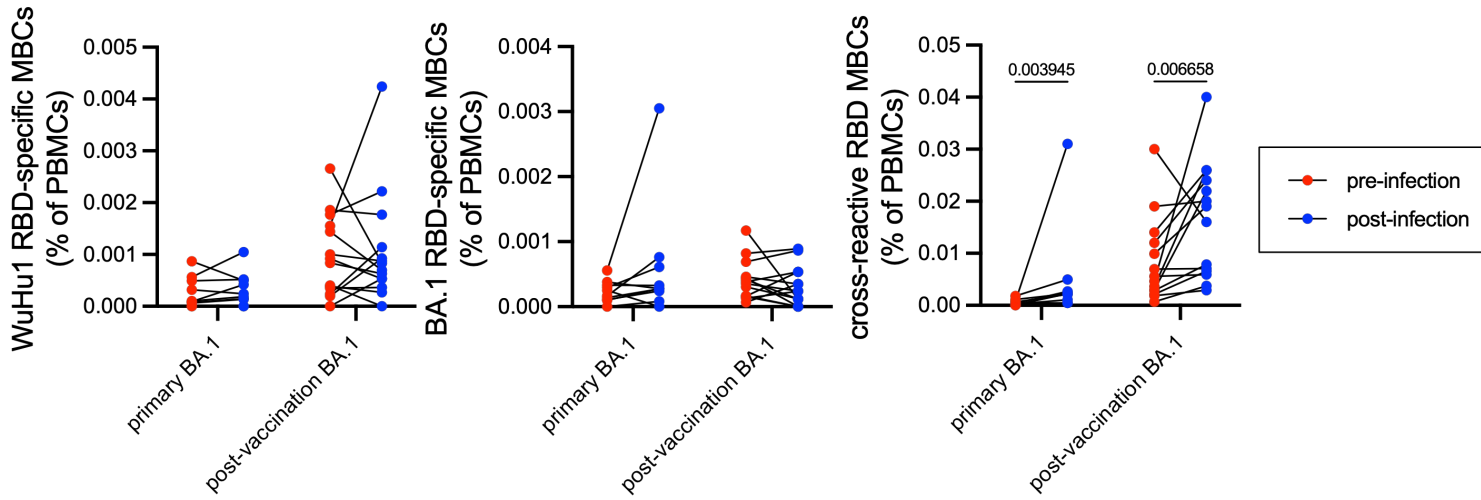


D.

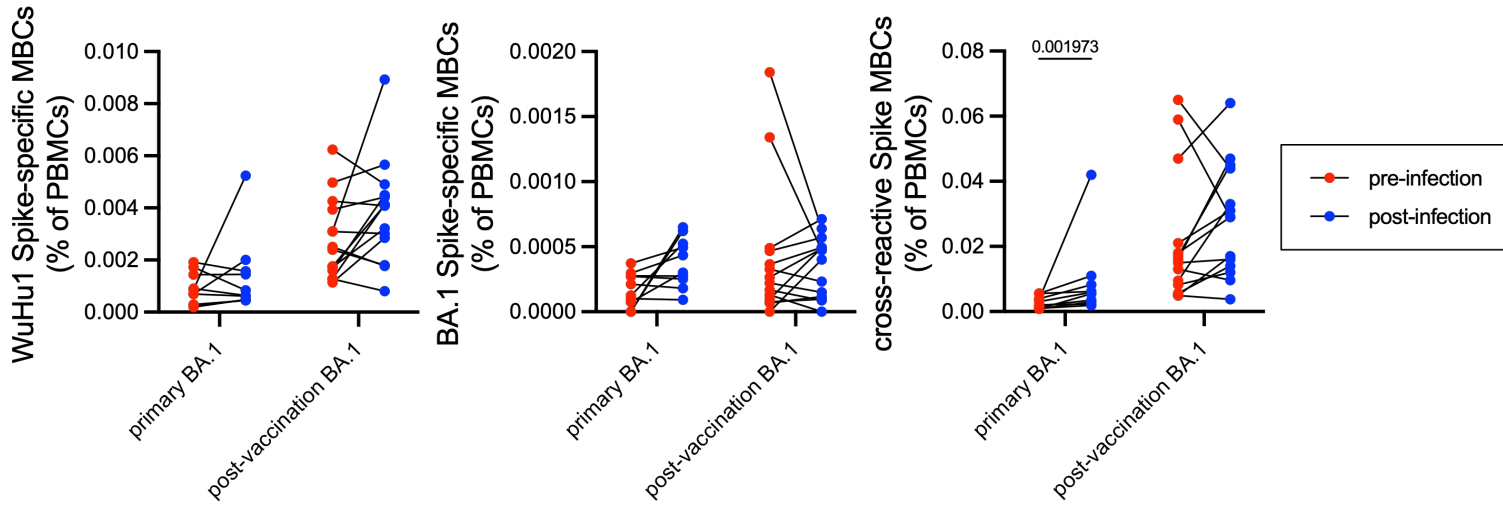


1227 **Figure 5. WuHu1 and BA.1 Memory B cell flow cytometric analysis and**  
1228 **quantification. (A)** Representative flow cytometric plots of WuHu1 and BA.1 RBD-  
1229 specific memory B cells (full gating strategy shown in Figure S3) in naïve, vaccinated  
1230 only, primary BA.1 infection, and post-vaccination BA.1 infection cohorts. Cells that bind  
1231 both WuHu1 RBD and BA.1 RBD are annotated as cross-reactive RBD+, whereas cells  
1232 that bind only WuHu1 RBD or BA.1 RBD are annotated as WuHu1 RBD+ or BA.1  
1233 RBD+, respectively. **(B)** Quantification of isotype-switched memory B cells for WuHu1  
1234 RBD+, BA.1 RBD+ and cross-reactive RBD+ specificities for each cohort of SARS-CoV-  
1235 2 immune histories. Each symbol represents an individual. Two-sided P values from t-  
1236 test statistics were calculated for pairwise differences using one-way ANOVA. Post hoc  
1237 testing for multiple comparisons between draws was performed using Tukey’s multiple  
1238 comparisons test. P values greater than 0.05 are not depicted. **(C)** Representative flow  
1239 cytometric plots of WuHu1 and BA.1 Spike-specific memory B cells (full gating strategy  
1240 shown in Figure S3) in naïve, vaccinated only, primary BA.1 infection, and post-  
1241 vaccination BA.1 infection cohorts. Cells that bind both WuHu1 RBD and BA.1 Spike  
1242 are annotated as cross-reactive Spike+, whereas cells that bind only WuHu1 Spike or  
1243 BA.1 Spike are annotated as WuHu1 Spike+ or BA.1 Spike+, respectively. **(D)**  
1244 Quantification of isotype-switched memory B cells for WuHu1 Spike+, BA.1 Spike+ and  
1245 cross-reactive Spike+ specificities for each cohort of SARS-CoV-2 immune histories.  
1246 Each symbol represents an individual. Two-sided P values from t-test statistics were  
1247 calculated for pairwise differences using one-way ANOVA. Post hoc testing for multiple  
1248 comparisons between draws was performed using Tukey’s multiple comparisons test. P  
1249 values greater than 0.05 are not depicted.

A.

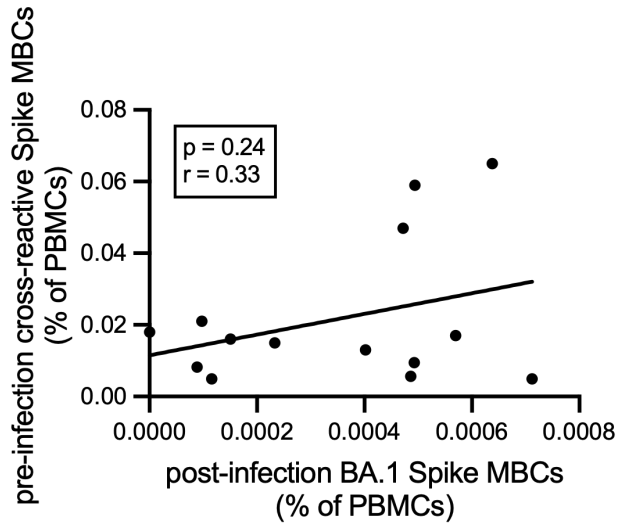


B.

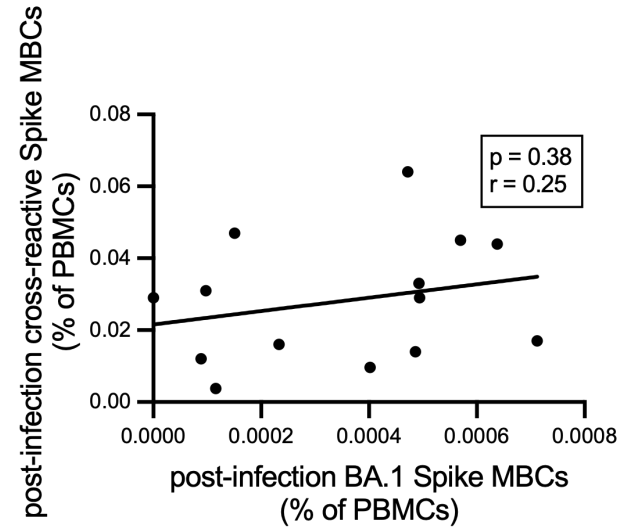


1250 **Figure 6. Frequency of WuHu1- and BA.1-specific memory B cells before and after**  
1251 **BA.1 infection. (A)** Frequencies of isotype-switched memory B cells with WuHu1  
1252 RBD+, BA.1 RBD+ and cross-reactive RBD+ specificities in both unvaccinated and  
1253 vaccinated individuals before and after BA.1 infection. Lines connect the same  
1254 individual from pre-infection frequency to post-infection frequency. In primary infections,  
1255 pre-infection blood draws were taken on average 75.6 days before infection and post-  
1256 infection blood draws occurred on 37.8 days after infection. In post-vaccination  
1257 infections, pre-infection blood draws were taken on average 87.6 days before infection  
1258 and post-infection draws were taken an average of 38.3 days after infection. Individuals  
1259 that received a vaccine after the pre-infection draw were excluded from analysis. P  
1260 values were calculated using Wilcoxon matched-pairs signed rank test on each row and  
1261 post hoc testing for multiple comparisons between draws was performed using two-  
1262 stage linear step-up procedure of Benjamini, Krieger and Yekutieli. P values greater  
1263 than 0.05 are not depicted. **(B)** Frequencies of isotype-switched memory B cells with  
1264 WuHu1 Spike+, BA.1 Spike+ and cross-reactive Spike+ specificities in both  
1265 unvaccinated and vaccinated individuals before and after BA.1 infection. Lines connect  
1266 the same individual from pre-infection frequency to post-infection frequency. P values  
1267 were calculated using Wilcoxon matched-pairs signed rank test on each row and post  
1268 hoc testing for multiple comparisons between draws was performed using two-stage  
1269 linear step-up procedure of Benjamini, Krieger and Yekutieli. P values greater than 0.05  
1270 are not depicted.  
1271  
1272

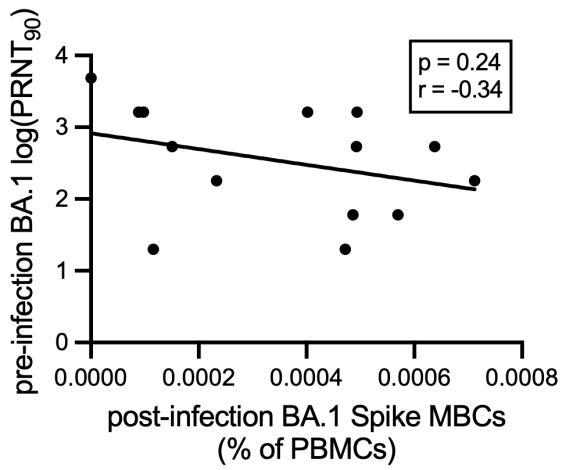
A.



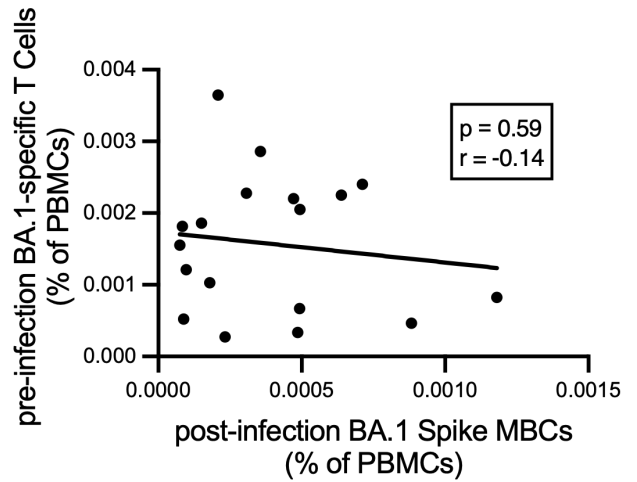
B.



C.

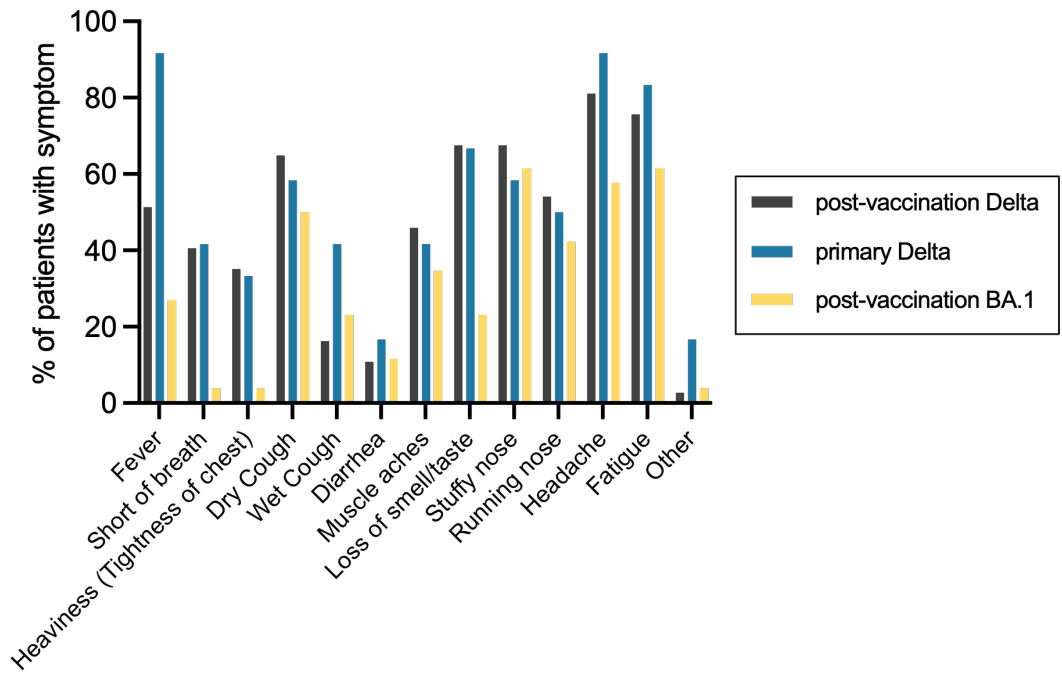


D.

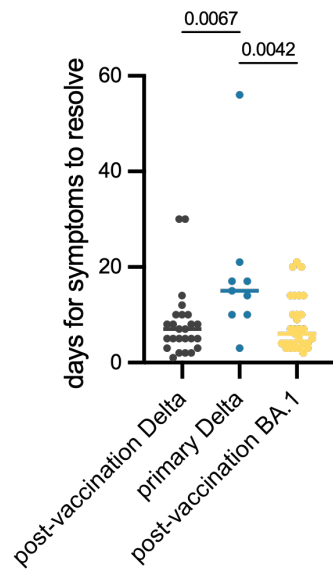


1273 **Figure 7. Correlations of pre-infection and post-infection BA.1-specific antibody,**  
1274 **T and B cell responses. (A)** Correlation of pre-infection cross-reactive Spike MBCs  
1275 (calculated as in Figure 5C) plotted against the frequency of post-infection BA.1 Spike  
1276 MBCs (calculated as in Figure 5C) in individuals that experienced a post-vaccination  
1277 BA.1 infection. Pearson correlation analysis was performed. Pre-infection blood draws  
1278 were taken on average 87.6 days before infection and post-infection draws were taken  
1279 an average of 38.3 days after infection. Individuals that received a vaccine after the pre-  
1280 infection draw were excluded from analysis. **(B)** Correlation of post-infection cross-  
1281 reactive Spike MBCs (calculated as in Figure 6B) plotted against the frequency of post-  
1282 infection BA.1 Spike MBCs (calculated as in Figure 5C) in individuals that experienced a  
1283 post-vaccination BA.1 infection. Pearson correlation analysis was performed. **(C)**  
1284 Correlation of pre-infection BA.1 neutralizing antibody titer (calculated as in Figure 4a)  
1285 plotted against post infection BA.1 Spike MBCs (calculated as in Figure 5c) in  
1286 individuals that experienced a post-vaccination BA.1 infection. Pearson correlation  
1287 analysis was performed. **(D)** Correlation of pre-infection BA.1 Spike-specific T cells as  
1288 measured by IFN $\gamma$  ELISPOTs plotted against post-infection BA.1 Spike MBCs in  
1289 individuals that experienced a post-vaccination BA.1 infection. Pearson correlation  
1290 analysis was performed.  
1291  
1292

**A.**



**B.**

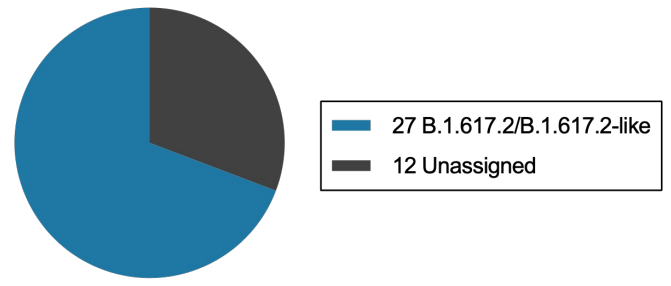


1293 **Figure S1. Test All, Test Smart (TATS) symptom report. (A)** Percentage of  
1294 individuals from each TATS cohort that reported experiencing various respiratory/cold  
1295 symptoms in study entry survey. **(B)** Reported days until symptoms resolved for each  
1296 TATS cohort. Two-sided P values from t-test statistics were calculated for pairwise  
1297 differences using one-way ANOVA. Post hoc testing for multiple comparisons between  
1298 draws was performed using Tukey's multiple comparisons test. P values greater than  
1299 0.05 are not depicted.  
1300



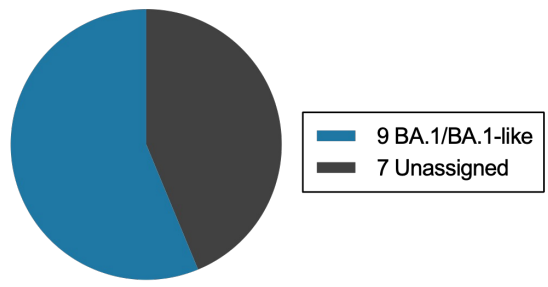
**A.**

TATS Delta cohort PANGO-lineages



Total=39

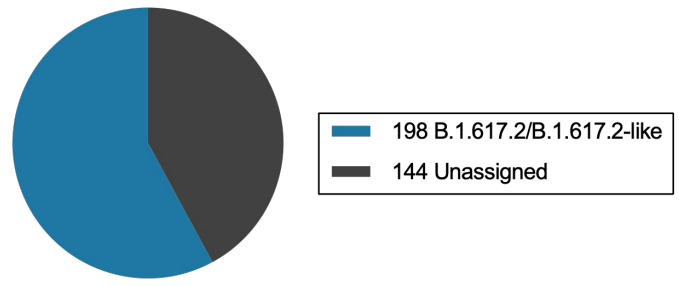
TATS BA.1 cohort PANGO-lineages



Total=16

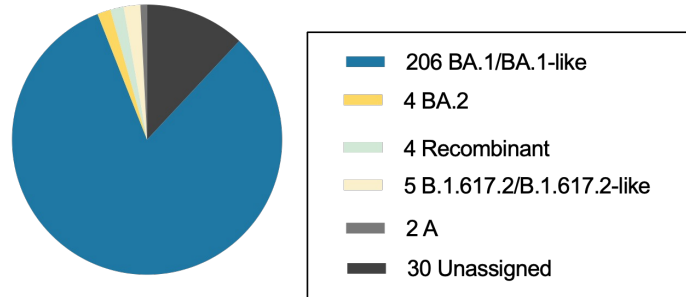
**B.**

TATS PANGO-lineages during Delta recruitment period (July 1, 2021-December 1, 2021)



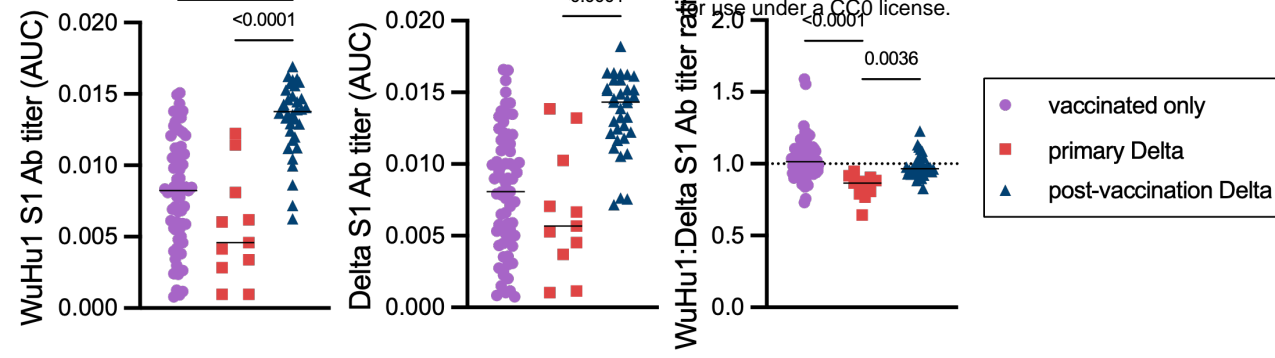
Total=342

TATS PANGO-lineages during BA.1 recruitment period (January 1, 2022 -March 31, 2022)



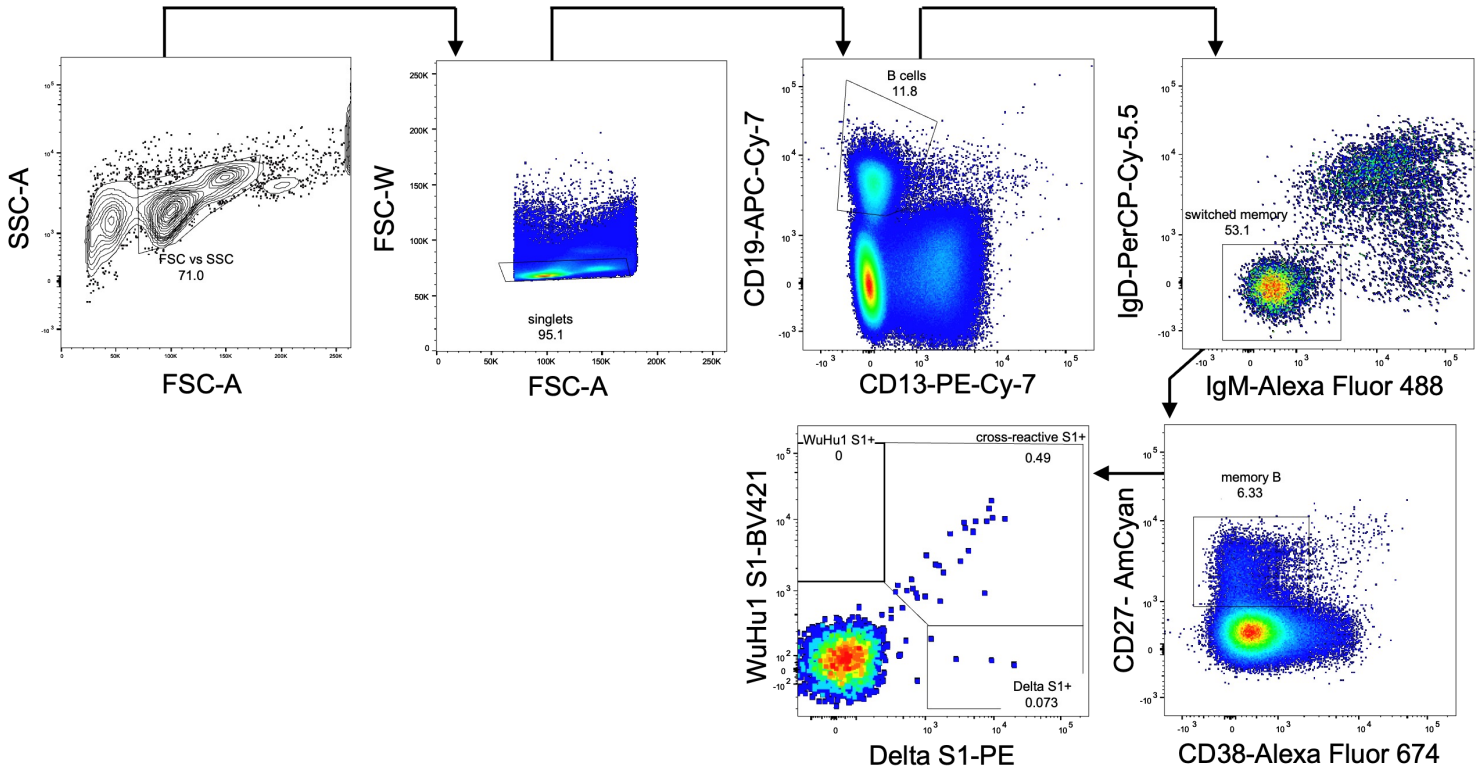
Total=251

1301 **Figure S2. PANGO-lineage assignments from TATS PCR positive individuals. (A)**  
1302 Delta or BA.1 PANGO-lineage assignments after SARS-CoV-2 viral amplicon  
1303 sequencing (Integrated DNA Technologies). Unassigned sequences could not be  
1304 assigned to a PANGO-lineage due to insufficient viral RNA recovery and low sequence  
1305 coverage. **(B)** PANGO-lineage assignments of all TATS samples submitted during the  
1306 period of Delta cohort recruitment, July 1, 2021-December 1, 2021 (left panel) or during  
1307 the period of BA.1 cohort recruitment, January 1, 2022-March 31, 2022 (right panel).  
1308 Unassigned sequences could not be assigned a lineage due to insufficient viral RNA  
1309 recovery and low sequence coverage.

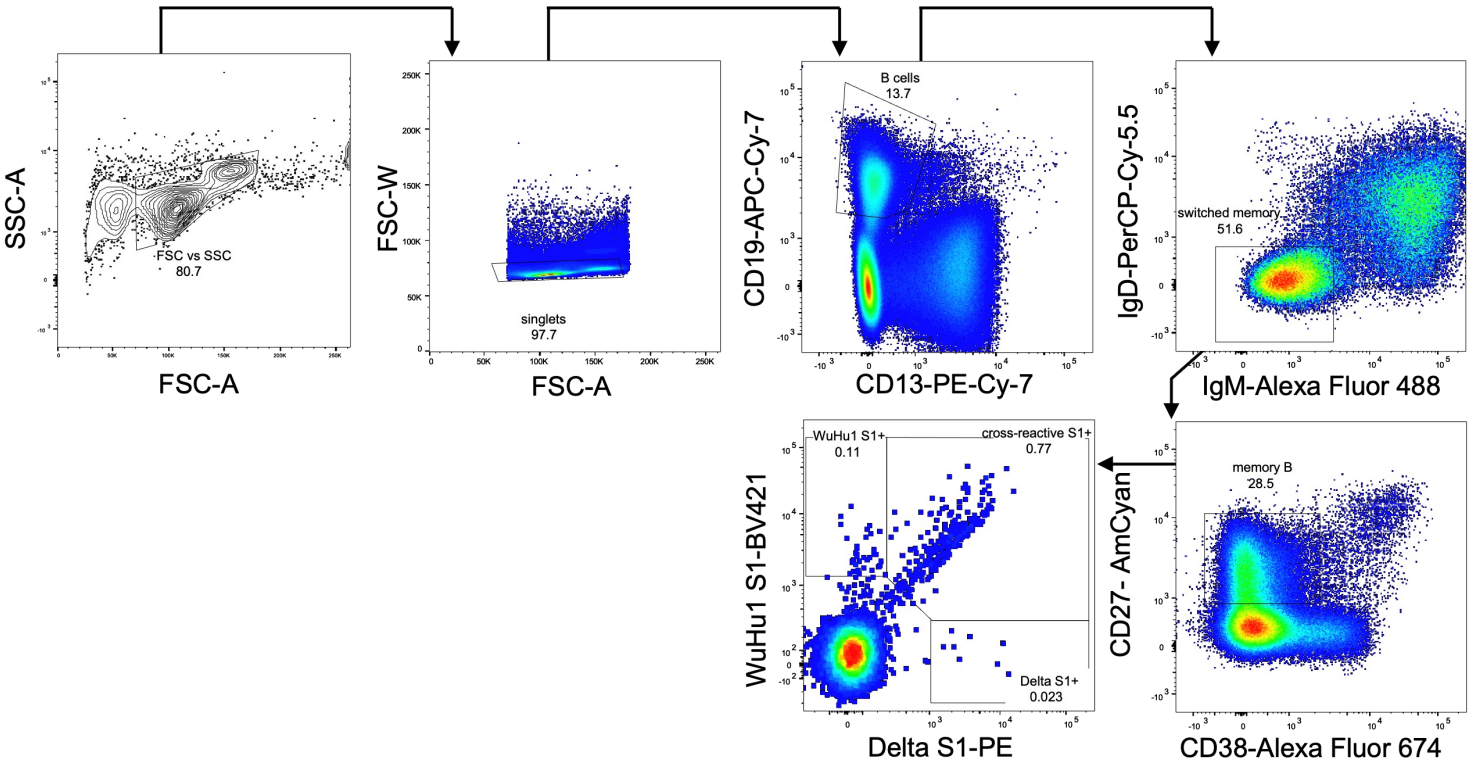


1310 **Figure S3. Primary and recall antibody responses to Wuhan and Delta strains of**  
1311 **SARS-COV-2.** Quantitative titers of WuHu1- and Delta S1-specific antibodies. Serum  
1312 was initially diluted 1:60, serially diluted 1:3, assessed by ELISA for binding to the listed  
1313 antigens, and area under the curve (AUC) values were calculated. Each symbol  
1314 represents an individual. WuHu1 AUC values were divided by their Delta AUC titer in  
1315 the same individual to calculate a WuHu1:Delta S1 ratio in the rightmost panel. Two-  
1316 sided P values from t-test statistics were calculated for pairwise differences using one-  
1317 way ANOVA. Post hoc testing for multiple comparisons between draws was performed  
1318 using Tukey's multiple comparisons test. P values greater than 0.05 are not depicted.  
1319  
1320  
1321  
1322

**primary Delta**

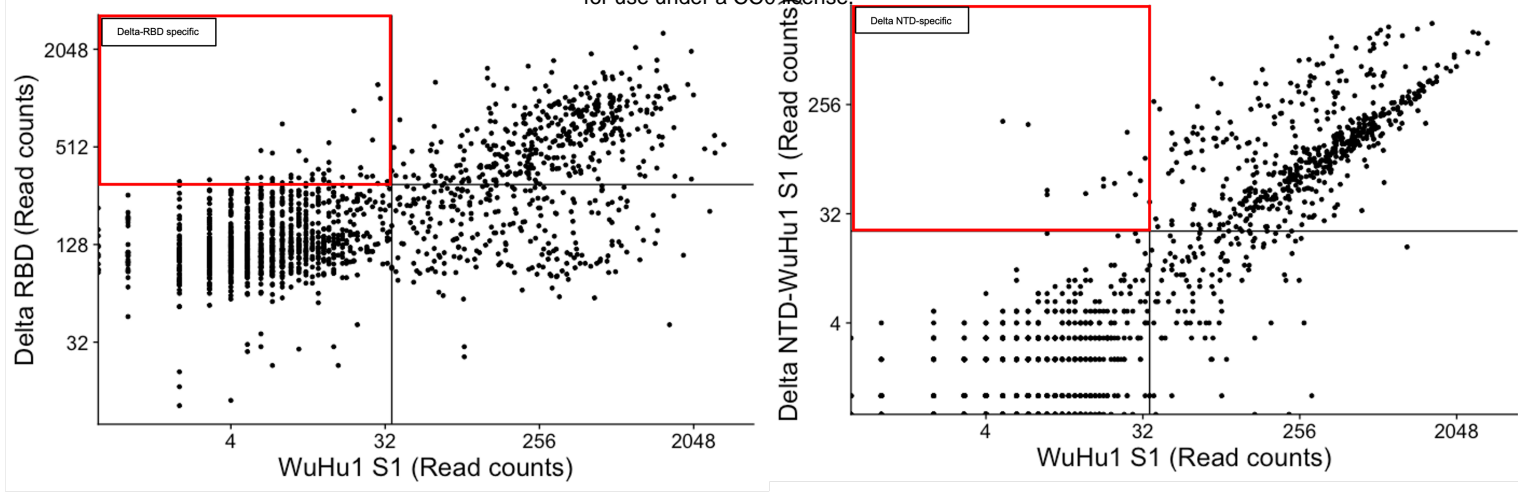


**post-vaccination Delta**

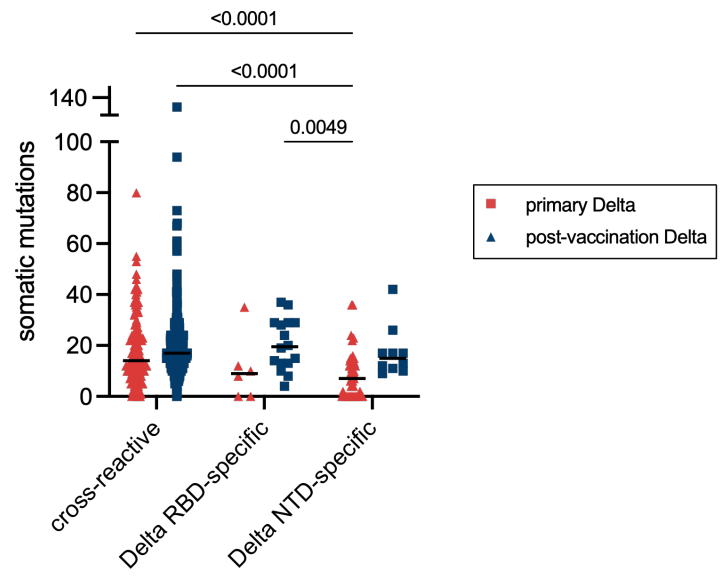


1323 **Figure S4. Flow cytometric gating strategy with Delta S1 and WuHu1 S1**  
1324 **tetramers.** Examples of a sample from a primary Delta infection (top) and post-  
1325 vaccination Delta infection (bottom) are shown.  
1326

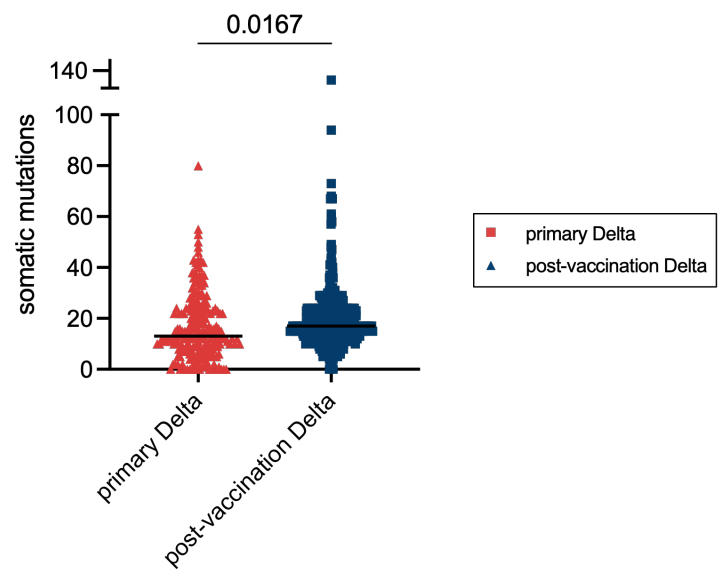
A.



B.



C.



1327 **Figures S5. LIBRA-seq analysis in post-vaccination Delta infections and**  
1328 **quantification of somatic mutations. (A)** A chimeric protein (Delta NTD-WuHu1 S1)  
1329 was generated in which Delta NTD mutated epitopes (T19R, G142D, E156-, F157-,  
1330 R158G) were incorporated into the otherwise WuHu1 S1 backbone. Quantification of  
1331 Delta RBD-specific (**left**) and Delta NTD-specific memory B cells (**right**) in individuals  
1332 that experienced a post-vaccination Delta infection. Delta RBD-specific cells were  
1333 classified by cells that had Delta RBD read counts of greater than 300 and WuHu1 S1  
1334 read counts of less than 35. Delta NTD-specific cells were classified by cells that had  
1335 Delta NTD-WuHu1 S1 read counts of greater than 23 and WuHu1 S1 read counts of  
1336 less than 35. Read count thresholds to determine positivity were set using samples in  
1337 which cells lacking Spike-binding specificities were sorted and sequenced. Plots are  
1338 concatenated from ten individuals. **(B)** Somatic mutations were calculated using the  
1339 observedMutations command in the Shazam Immcantation package in R. Specificities  
1340 of cells are determined using the same cutoffs described in **Figure S3A and 3D. (C)**  
1341 Quantification of somatic mutations of all Spike specific cells subjected to scRNAseq  
1342 from either ten post-vaccination or primary Delta infections.

1343

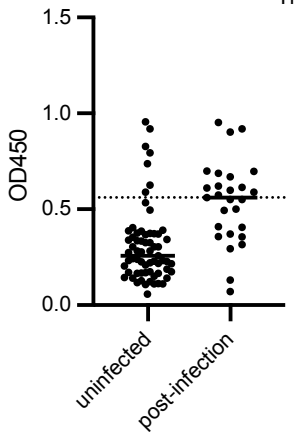
1344

1345

1346

1347

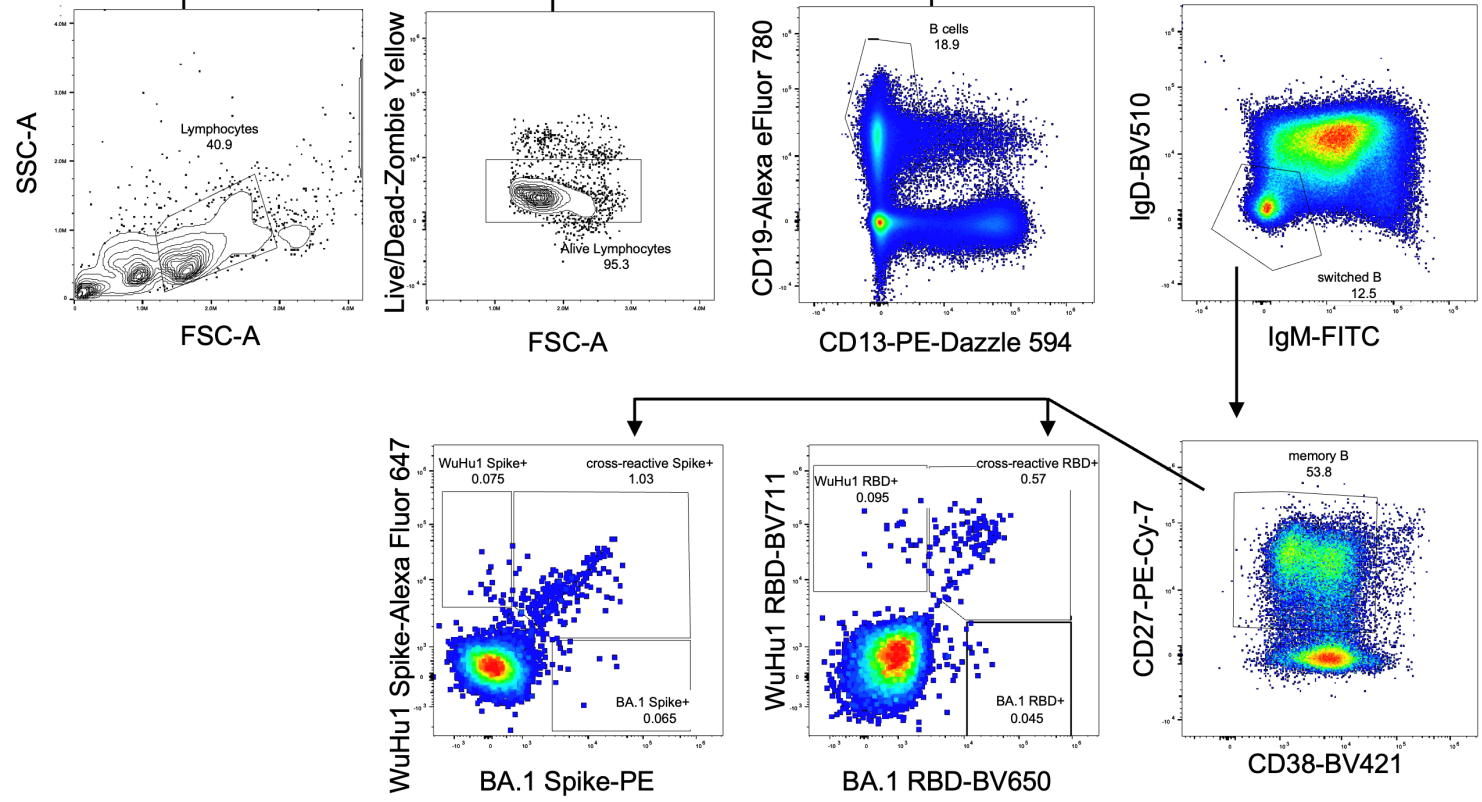




1348 **Figure S6. anti-Nucleocapsid titers in uninfected individuals.** Individuals with  $\alpha$ -  
1349 Nucleocapsid titers of greater than 0.6 at a 1:60 serum dilution were considered  
1350 previously infected and excluded from the study.

1351

1352



1353 **Figure S7. Flow cytometric gating strategy with BA.1 RBD, BA.1 Spike, WuHu1**

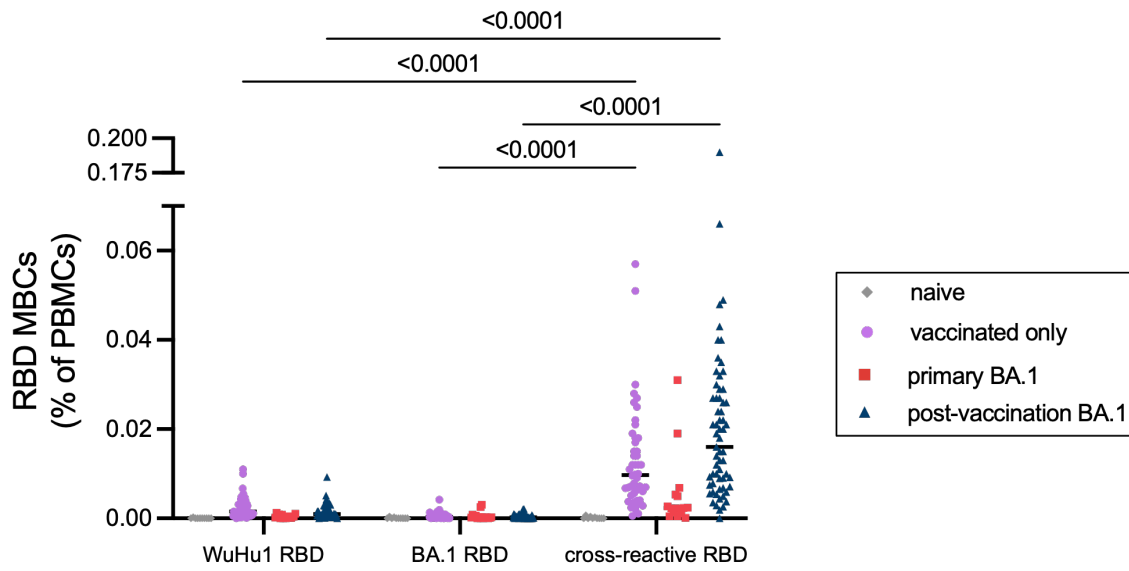
1354 **RBD and WuHu1 Spike tetramers.** An example of a sample from a post-vaccination

1355 BA.1 infection is shown.

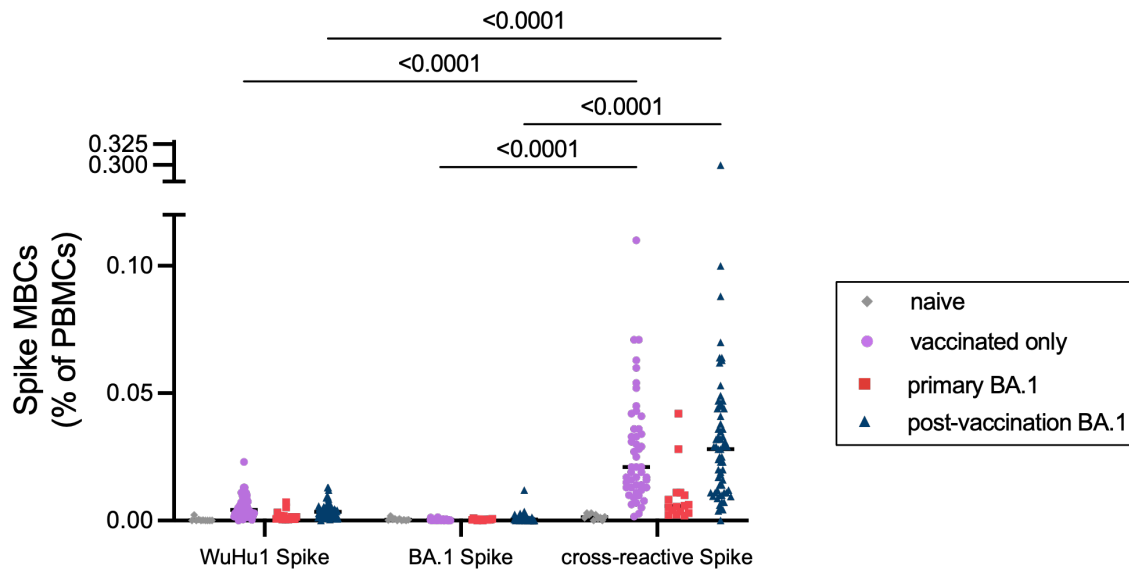
1356

1357

A.



B.



1358 **Figure S8. WuHu1 and BA.1 Memory B cell flow cytometric quantification. (A)**  
1359 Cells that bind both WuHu1 RBD and BA.1 RBD are annotated as cross-reactive RBD+,  
1360 whereas cells that bind only WuHu1 RBD or BA.1 RBD are annotated as WuHu1 RBD+  
1361 or BA.1 RBD+, respectively. Quantification of isotype-switched memory B cells as a  
1362 percentage of total PBMCs for WuHu1 RBD+, BA.1 RBD+ and cross-reactive RBD+  
1363 specificities for each cohort of SARS-CoV-2 immune histories. Each symbol represents  
1364 an individual. Two-sided P values from t-test statistics were calculated for pairwise  
1365 differences using two-way ANOVA. Post hoc testing for multiple comparisons between  
1366 draws was performed using Tukey's multiple comparisons test. P values greater than  
1367 0.05 are not depicted. **(B)** Cells that bind both WuHu1 RBD and BA.1 Spike are  
1368 annotated as cross-reactive Spike+, whereas cells that bind only WuHu1 Spike or BA.1  
1369 Spike are annotated as WuHu1 Spike+ or BA.1 Spike+, respectively. Quantification of  
1370 isotype-switched memory B cells for WuHu1 Spike+, BA.1 Spike+ and cross-reactive  
1371 Spike+ specificities for each cohort of SARS-CoV-2 immune histories. Each symbol  
1372 represents an individual. Two-sided P values from t-test statistics were calculated for  
1373 pairwise differences using two-way ANOVA. Post hoc testing for multiple comparisons  
1374 between draws was performed using Tukey's multiple comparisons test. P values  
1375 greater than 0.05 are not depicted.  
1376

	<b>vaccinated only (statewide antibody testing initiative) (n=74)</b>	<b>primary Delta (n=12)</b>	<b>post-vaccination Delta (n=37)</b>	<b>vaccinated only (TATS) (n=62)</b>	<b>primary BA.1 (n=69)</b>	<b>post- vaccination BA.1 (n=62)</b>
<b>Age</b> Mean (s.d.)	38.0 (32.0, 54.0)	21.9 (20.2, 40.7)	23.3 (18.6, 65.8)	31.9 (18.6, 65.0)	44 (25, 62)	40 (19, 71.5)
<b>Sex</b>						
Male	22 (32%)	5 (42%)	8 (22%)	24 (39%)		24 (39%)
Female	52 (68%)	7 (58%)	29 (78%)	37 (60%)		34 (55%)
<b>Prior COVID infection</b>						
Yes		12 (100%)	37 (100%)		69 (100%)	64 (100%)
No	74 (100%)					
Time since COVID infection paired pre- and post- infection samples		67.5 days (32, 99.3)	71.5 days (48.5, 89.5)		40 days (31, 44.5) 10	54.4 days (34.5, 71) 21
Time from vaccination to pre- infection draw						138 (32.5, 217)
Time from pre- infection draw to infection					73.3 days (30, 99)	112 days (33, 187)
Time from infection to post- infection draw					42.7 days (29.5, 47.5)	44.8 days (34, 49.3)
<b>COVID Vaccination # of shots</b>	37	0	37	62	0	62
2	37 (100%)		37 (100%)	16 (26%)		13 (20%)
3				46 (74%)		15 (23%)
4						3 (5%)
time since vaccination	135.6 days (126, 270)		273.9 days (56, 317)	176.0 days (113.5, 188)		192.2 days (107, 302.3)

1377 **Table 1. Characteristics of cohorts**

1378 Interquartile range (IQR) is listed in parentheses unless otherwise stated in the table.

1379